photochem

MDPI

Review

Recent Advances in Visible Light Photoinitiating Systems Based on Flavonoids

Frédéric Dumur

Aix Marseille Univ, CNRS, ICR, UMR 7273, F-13397 Marseille, France; frederic.dumur@univ-amu.fr

Abstract: The design of biosourced and/or bioinspired photoinitiators is an active research field as it offers a unique opportunity to develop photoinitiating systems exhibiting better biocompatibility as well as reduced toxicity. In this field, flavonoids can be found in numerous fruits and vegetables so these structures can be of interest for developing, in the future, polymerization processes, offering a reduced environmental impact but also better biocompatibility of the polymers. In this review, the different flavonoids reported to date as photoinitiators of polymerization are presented. Over the years, different modifications of the flavonoid scaffold have been examined including the grafting of well-known chromophores, the preparation of Type II photoinitiators or the introduction of photocleavable groups enabling the generation of Type I photoinitiators. Different families of flavonoids have also been investigated, enabling to design of high-performance photoinitiating systems.

Keywords: photoinitiator; visible light; photopolymerization; LED; flavonoids; natural products

check for updates

Citation: Dumur, F. Recent Advances in Visible Light Photoinitiating Systems Based on Flavonoids. *Photochem* **2023**, *3*, 495–529. https://doi.org/10.3390/photochem3040030

Academic Editor: Anna Cleta Croce

Received: 28 September 2023
Revised: 28 November 2023
Accepted: 4 December 2023
Published: 12 December 2023

1. Introduction

Photopolymerization is an active research field. Nowadays, tremendous efforts are devoted to developing highly efficient photoinitiating systems activable under visible light. Indeed, photopolymerization is used in a wide range of applications of photopolymerization from coatings and varnishes, adhesives, solvent-free paints and dental restoration materials to 3D/4D printing and microelectronics [1–15]. If the reactivity of photoinitiators remains the main parameter governing the design of new structures, their toxicities and biocompatibilities are more and more regarded [16–19]. Indeed, for applications such as food packaging and different bioapplications, the toxicity of the final polymers and more generally the final composites (obtained by the introduction of fillers in polymers) is of crucial importance. Therefore, a good balance between toxicity and reactivity has to be found [16,20–26]. For decades, a great deal of effort has been devoted to developing greener photopolymerization processes, consisting in the use of biosourced photoinitiators and/or biosourced monomers [27–29], the use of sunlight instead of artificial light to initiate the polymerization [30–35] or the development of water-soluble photoinitiating systems enabling to avoid the use of organic solvents [36–39]. In order to identify the appropriate scaffold for designing high-performance visible light photoinitiators, a wide range of structures have been screened over the years, as exemplified with diketopyrrolopyrroles [40], bodipy [41–46], perylenes [47], dithienophosphole derivatives [48], thiophenes [49], cyclohexanones [50–52], quinoxalines [53–66], glyoxylates [67], cyanines [68], benzylidene ketones [69–73], phenothiazines [74], iodonium salts [75–81], naphthalimides [82–85], triphenylamines [86–88], photochroms [89], pyridinium salts [90], helicenes [91], silane, germane and stannane [92,93], push–pull dyes [32,33,94,95], acridine-1,8-diones [96], zinc complexes [97], biosourced photoinitiators [98], copper complexes [99–103], iron complexes [104,105], thioxanthones [37,41,106–118], furan derivatives [119], camphorquinone [120,121], anthracenes [122], benzophenones [123,124], chalcones [125–131], terphenyls [132], phenacyl bromide [133], NIR dyes [134], pyrenes [135–137], carbazoles [138–142], coumarins [143–146], gold complexes [147] and iridium complexes [148]. Natural compounds were also examined as photoinitiators of polymerization such as curcumin [149–152], different anthraquinones [153–155]

or naphthoquinones [156]. Flavonoids that can be found in numerous fruits and vegetables [157–165], but also in plant products such as chocolate, tea and wine, were identified as promising candidates for the design of visible light photoinitiators. Flavonoids are a family of compounds including more than six thousand low-molecular-weight phenolic compounds derived from flavan [166].

Flavonoids are composed of nine main subgroups including flavones, flavonols, flavanols, flavononols, flavonones, isoflavones, anthocyanines, neoflavonoids and chalcones (see Figure 1). Plants clearly constitute an inexhaustible source of flavonoids on earth.

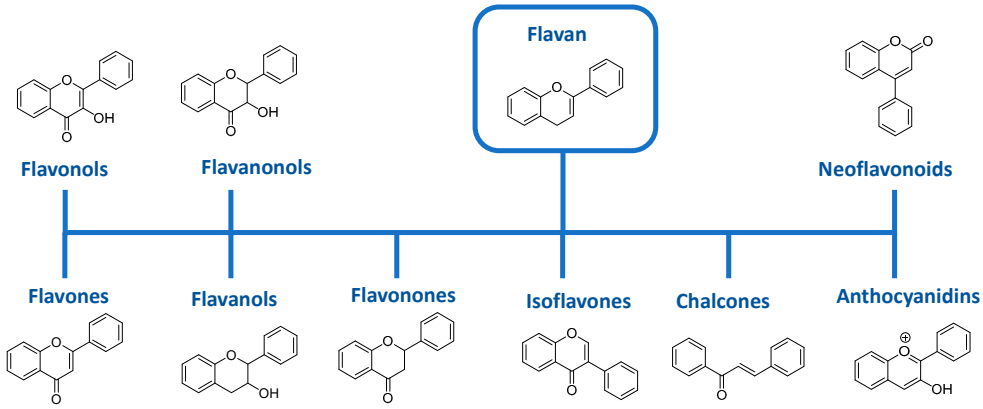

Figure 1. The different subgroups of flavonoids.

Flavonoids are extensively used in the biomedical field, due to their anti-oxidative, anti-inflammatory, anti-mutagenic, anti-carcinogenic and anti-diabetic properties [167–169]. Flavonoids are important therapeutic agents used in a variety of heath disorders including hypoglycemia, cancer, chronic inflammation or cardiovascular complications [170,171]. These natural dyes are also used in food and cosmetic industries since these structures can be used as pigments and biopreservatives [172]. Among flavonoids, chalcones have been extensively studied as visible light photoinitiators of polymerization due to their easiness of synthesis, low cost and chemical stability [173,174]. The other subgroups of flavonoids have been less studied, attributable to more difficult synthetic routes and the low availability of these structures in nature, inducing high costs for the commercially available flavonoids and thus drastically limiting their potential use as photoinitiators for the industrial production of polymers. In addition, numerous structures have been identified as interesting scaffolds for the design of Type I and Type II photoinitiators. Indeed, photoinitiators can be divided into two main groups, namely Type I photoinitiators, which are monocomponent systems and can generate radicals by homolytic cleavage of a specific bond [175–177], and parallel to this, Type II photoinitiators, which can only generate initiating species by means of a multi-step reaction mechanism when combined to a hydrogen donor or an electron acceptor/donor. The first flavonoids to be studied as visible light photoinitiators were flavonols which could efficiently promote the cationic polymerization (CP) of epoxides upon irradiation with a laser diode emitting at 457 nm but also in soft irradiation conditions with an LED emitting at 462 nm [178]. Following this work, various flavonoids were studied, paving the way toward biosourced or bioinspired photoinitiators. In this review, an overview of the different flavonoids examined as visible light photoinitiators of polymerization is given.

2. Flavonoids as Visible Light Photoinitiators

2.1. Flavonols

Flavonols have been extensively studied in health sciences, due to their low toxicities but also due to their antioxidant and anticancer activities [179–187]. Flavonols also possess excellent optical properties [188–192]. Due to the presence of the hydroxy group close to the ketone group, these dyes also exhibit excited state intramolecular proton transfer (ESIPT)

properties, enabling these dyes to have large Stokes shifts and a dual emission associated with the formation of two excited states, the first one corresponding to the Franck–Condon excited state and the second one attributed to the tautomeric form issued from ESIPT [193–205]. Despite these appealing features, several drawbacks can be cited, especially regarding the stability of flavonols under light irradiation. In addition to the aforementioned intramolecular proton transfer [193–196,206–211], photooxidation [212–214], reverse proton transfer [215] or photorearrangement reaction [216,217] can be cited as the main photoinduced chemical reactions. Despite this attested instability under irradiation, flavonols were used in photopolymerization. Notably, the remarkable fluorescence of a flavonol derivative was used for the real-time monitoring of the FRP of an acrylate-based E-Shell 300 biocompatible polymer by using the flavanol derivative as a fluorescent probe. However, this flavonol derivative was not used as a photoinitiator/photosensitizer but only as a probe [205].

The first report mentioning the use of flavonoids as photoinitiators of polymerization was reported in 2013 by Lalevée and coworkers [178]. In order to provide sufficient absorption in the visible range, different chromophores were connected to the flavonol scaffold, namely pyrene, anthracene or a *para*-dimethylaminophenyl group (see Figure 2).

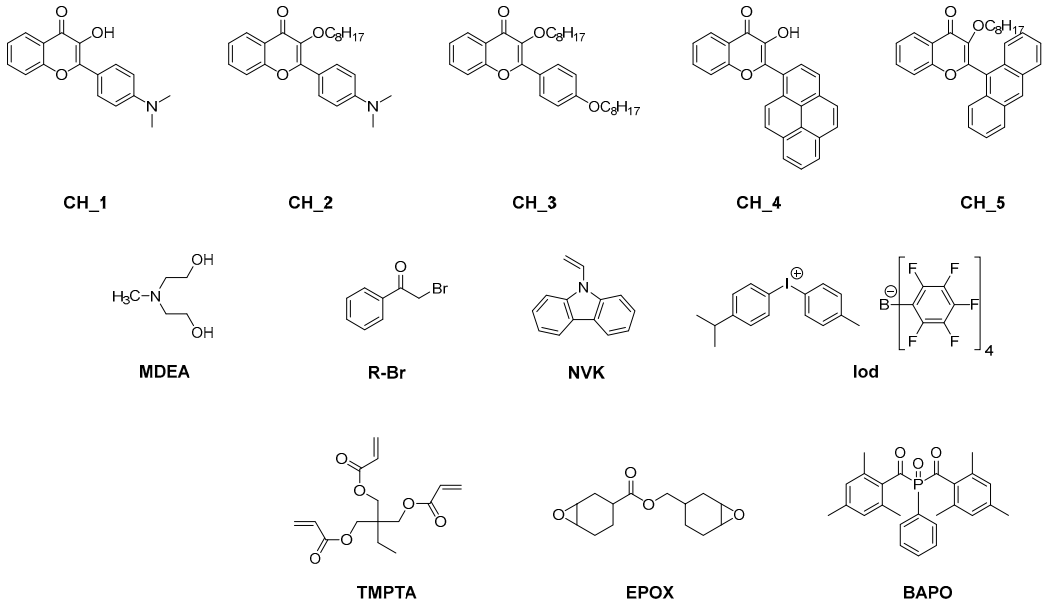

Figure 2. Chemical structures of flavonols CH_1-CH_5, different monomers and additives.

From the absorption viewpoint, modification of the side groups strongly impacted the absorption properties of the dyes. All dyes exhibited an absorption maximum located in the near-UV-visible range, except for CH_4 for which an absorption maximum located at 431 nm was determined in acetone. In the case of CH_1-CH_3 and CH_5, maxima located at 394, 377, 325 and 385 nm were respectively measured in acetonitrile. Noticeably, alkylation of the phenolic group in CH_1 blueshifted the absorption of CH_2 by ca. 17 nm, from 394 nm for CH_1 up to 377 nm for CH_2. Improvement in the electron-donating ability of the side group contributed to the redshift of the absorption, as exemplified with CH_2 exhibiting an absorption redshifted by ca. 50 nm compared to CH_3 bearing a weak electron donor (See Figure 3). Considering that the absorption of all dyes extends until the visible range, these dyes were thus appropriate candidates for polymerization experiments performed at 457 nm with a laser diode (I = 100 mW/cm^2), at 462 nm with an LED (I = 15 mW/cm^2) and upon irradiation with a halogen lamp (370–800 nm range, I = 12 mW/cm^2). Two different mechanisms were investigated, an oxidative and a reductive pathway. Among the two possible mechanisms, the oxidative pathway proved to be the most reactive one. By using the three-component dye/Iod/NVK systems (where Iod and NVK respectively stand for [methyl-4-phenyl-(methyl-1-ethyl)-4-phenyl]iodonium

tetrakis(pentafluorophenyl)borate and *N*-vinylcarbazole), the phenyl radicals formed by photoinduced electron transfer from the excited dye toward the electron-deficient iodonium salt can further react with NVK, producing Ph-NVK$^{\bullet}$. These radicals can also react with Iod, generating Ph-NVK^{+} [97,218,219]. Therefore, this mechanism can contribute to promoting both the free radical polymerization (FRP) of acrylates and the free-radical-promoted cationic polymerization (FRPCP) of epoxides (see Equations (r1)–(r3)). By UV-visible absorption spectroscopy, the formation of CH_1$^{\bullet+}$ could be detected at ca. 500 nm, supporting the oxidation step. The formation of CH_1$^{\bullet+}$ and Ph$^{\bullet}$ was also evidenced by electron spin resonance (ESR).

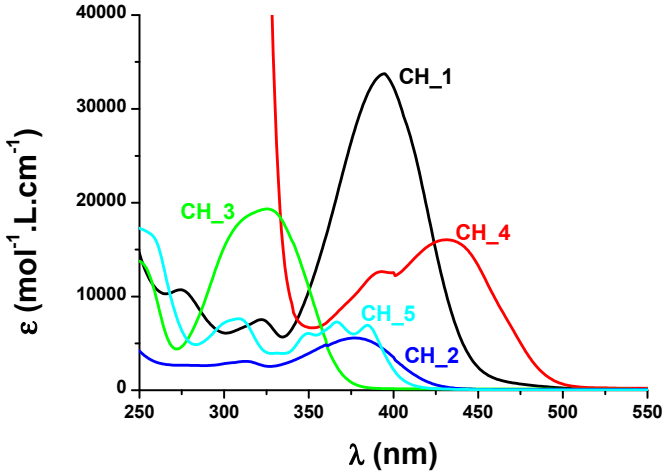

Figure 3. UV-visible absorption spectra of CH_1–CH_5 in acetonitrile, except CH_4 in acetone. Reproduced with permission from Ref. [178]. Copyright 2013, Royal Society of Chemistry.

$$CH \rightarrow {}^{1}CH\ (h\nu)$$

$$^{1}CH + Ph_2I^{+} \rightarrow CH^{\bullet+} + Ph_2I^{\bullet} \text{ and } Ph_2I^{\bullet} \rightarrow Ph^{\bullet} + Ph\text{-}I \quad (r1)$$

$$Ph^{\bullet} + NVK \rightarrow Ph\text{-}NVK^{\bullet} \quad (r2)$$

$$Ph\text{-}NVK^{\bullet} + Ph_2I^{+} \rightarrow Ph\text{-}NVK^{+} + Ph\text{-}I + Ph^{\bullet} \quad (r3)$$

In the case of the three-component dye/MDEA/R-Br system (where MDEA and R-Br stand for *N*-methyldiethanolamine and phenacyl bromide), the formation of phenacyl radicals could be identified as the unique radicals formed with this three-component system during the ESR experiments (see Equations (r4) and (r5)).

$$^{1}CH + MDEA \rightarrow CH^{\bullet-} + MDEA^{\bullet+} \quad (r4)$$

$$CH^{\bullet-} + R\text{-}Br \rightarrow CH + R^{\bullet} + Br^{-} \quad (r5)$$

Examination of the photoinitiating abilities of CH_1–CH_5 during the CP of (3,4-epoxycyclohexane)methyl 3,4-epoxycyclohexylcarboxylate (EPOX) upon irradiation with a halogen lamp revealed CH_1 to outperform the other dyes. Thus, a conversion of 60% after 800 s of irradiation was determined, contrarily to 30–40% for CH_2-CH_5 in the same conditions (see Figure 4). Using CH_1 as the chromophore, a slightly higher EPOX conversion was determined at 457 nm (65% conversion vs. 60% with the halogen lamp).

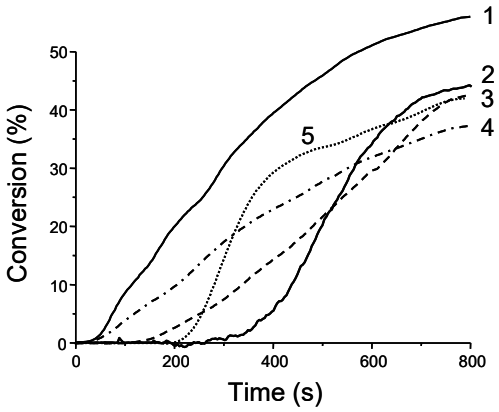

Figure 4. Photopolymerization profiles of EPOX under air upon irradiation with a halogen lamp using the three-component dye/NVK/Iod (0.5%/3%/3% *w*/*w*) system with (1) CH_1; (2) CH_4; (3) CH_3; (4) CH_2; (5) CH_5. Reproduced with permission from Ref. [178]. Copyright 2013, Royal Society of Chemistry.

Comparison with the reference three-component phenyl*bis*(2,4,6-trimethylbenzoyl) phosphine oxide (BAPO)/Iod/NVK system revealed CH_1 to furnish similar monomer conversions to BAPO in three-component systems. While examining the FRP of trimethylolpropane triacrylate (TMPTA) using the reductive pathway, only CH_1 and CH_2 could furnish acceptable monomer conversions (see Figure 5). If no monomer conversion could be detected with the two-component CH_1 or CH_2/MDEA systems, a conversion of ca. 40 and 35% could be obtained after 300 s of irradiation with a halogen lamp using the three-component CH_1/MDEA/R-Br (0.5%/4%/3% *w*/*w*) and CH_2/MDEA/R-Br (0.5%/4%/3% *w*/*w*) systems. This conversion could be significantly increased by using a laser diode emitting at 457 nm. In these conditions, a conversion of 60% could be determined using the three-component CH_1/MDEA/R-Br (0.5%/4%/3% *w*/*w*) system. Comparison with the reference two-component Eosin-Y/MDEA (0.1%/3% *w*/*w*) system (30% conversion after 300 s) revealed the two three-component systems based on CH_1 and CH_2 to outperform the reference system. Considering that cations and radicals are both formed with the three-component CH_1/Iod/NVK system, the elaboration of interpenetrated polymer networks by the concomitant polymerization of TMPTA and EPOX was examined under air. After 1000 s of irradiation at 457 nm with a laser diode, photopolymerization of a TMPTA/EPOX blend (50%/50%) under air furnished tack-free polymers. Using low light intensities (LED@462 nm and a halogen lamp), 30 min. was required to get tack-free coatings.

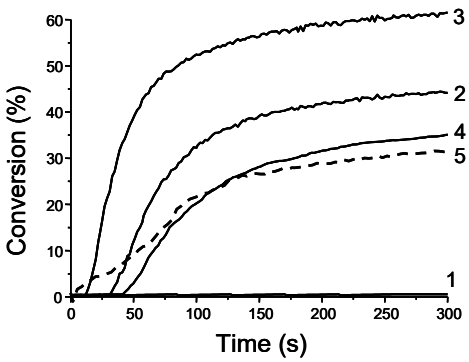

Figure 5. Photopolymerization profiles of TMPTA in laminated conditions upon exposure to (1) a halogen lamp or laser diode (457 nm) in the presence of CH_1/MDEA (0.5%/4% *w*/*w*); (2) a halogen lamp in the presence of CH_1/MDEA/R-Br (0.5%/4%/3% *w*/*w*); (3) the laser diode in the presence of CH_1/MDEA/R-Br (0.5%/4%/3% *w*/*w*); (4) a halogen lamp in the presence of CH_2/MDEA/R-Br (0.5%/4%/3% *w*/*w*); (5) a halogen lamp in the presence of Eosin-Y/MDEA (0.1%/3% *w*/*w*). Reproduced with permission from Ref. [178]. Copyright 2013 Royal Society of Chemistry.

In 2016, the first natural flavonoid dye, namely quercetin (3,5,7,3′,4′-pentahydroxyflavone), was examined by Versace and coworkers both as a photosensitizer and an antibacterial agent for the design of antibacterial coatings (see Figure 6) [220]. Indeed, an efficient strategy to cause the apoptosis of bacteria consists in producing reactive oxygen species (ROS) that will be capable of degrading cells [221–224]. Among ROS, singlet oxygen constitutes the best approach to prevent microorganism adhesion and proliferation on any surface. Prior to this work, several photoinitiators of polymerization have been identified as providing antimicrobial properties to coatings such as hydroxyethyl Michler's ketone [225], rose Bengal [226,227], porphyrins and phthalocyanines [228,229], eosin Y [226,230], toluidine blue [231] or methylene blue [231–233]. If these synthetic dyes showed interesting properties, a step further consists in using natural dyes to act as antibacterial agents, which constitutes a major environmental challenge. Quercetin was selected as the dye in this study as this flavonoid is among the most abundant ones in nature [234–239]. It can notably be found in numerous fruits and vegetables (onion, lemon, apple, grape, tomato, etc.), different beverages such as tea and red wine and even olive oil [240–242].

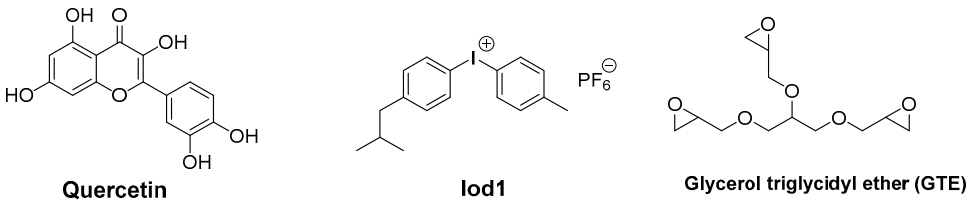

Figure 6. Chemical structures of quercetin, Iod1 and the biosourced monomer GTE.

Quercetin also exhibits antiviral, anti-inflammatory, anti-allergic and antioxidant activities, and this natural compound is also beneficial to limit cancer risks and cardiovascular problems [243–245]. Considering that quercetin is responsible for the green color of oak leaves, an absorption extending up to 430 nm was determined in acetonitrile, with an absorption maximum at 370 nm (ε = 19,000 $M^{-1}\cdot cm^{-1}$). An emission peak was also determined at 535 nm so that a Stokes shift of 8350 cm^{-1} could be calculated (see Figure 7). This large Stoke shift is indicative of a significant electronic change between the ground state and the excited state. Photolysis experiments performed with the two-component quercetin/Iod1 system revealed the photogeneration of Bronsted acid (H^+) using rhodamine B as an acid indicator. Quercetin was thus identified as a promising candidate for CP.

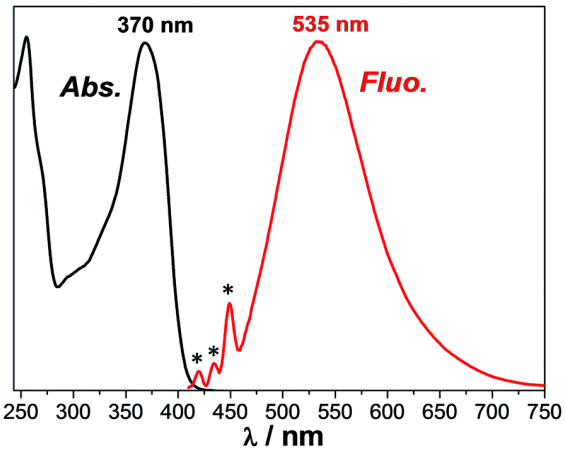

Figure 7. UV-visible absorption and fluorescence spectra of quercetin in acetonitrile. Raman scattering peaks of acetonitrile are indicated by asterisks (*). Reproduced with permission from Ref. [220]. Copyright 2016, Royal Society of Chemistry.

Using glycerol triglycidyl ether (GTE) as the monomer and upon irradiation with a Xe lamp (I = 70 mW/cm^2), a GTE conversion of 75% could be determined after 1200 s of irradiation using the two-component quercetin/Iod1 (2.5%/4% *w*/*w*) system (where Iod1 stands for 4-(2-methylpropyl)phenyl iodonium hexafluorophosphate). Interestingly, the quercetin-based coatings exhibited remarkable thermal stability since a decomposition temperature higher than 375 °C could be determined by thermogravimetric analysis (TGA). Examination of the fluorescence of the polymer films revealed the presence of remaining quercetin that could be advantageously used to generate reactive oxygen species upon light activation. Antibacterial properties were examined with Gram-negative bacteria (*E. coli*) and Gram-positive bacteria (*S. aureus*). Noticeably, quercetin-based coatings only exhibited antiproliferation properties for Gram-positive bacteria. In the case of *E. coli*, the development of bacteria was neither inhibited by light nor affected by the presence of quercetin within the polymer film. On the contrary, a total death of Gram-positive bacteria (*S. aureus*) was determined after 2 h of irradiation. The insensitivity of Gram-negative bacteria to singlet oxygen was assigned to the presence of lipopolysaccharides in the cell wall offering some protection against exogenous agents.

More recently, quercitin and morin, which are two isomers of position, were compared for their photoinitiating abilities during the FRP of a BisGMA/TEGDMA (1/1) blend (where BisGMA and TEGDMA stand for bisphenol A-glycidyl methacrylate and triethylene glycol dimethacrylate, respectively) or TMPTA, the cationic polymerization of tri(ethylene glycol) divinyl ether (DVE-3), and the polymerization thiol-ene of a DVE-3/trimethylolpropane *tris*(3-mercaptopropionate) (Trithiol) (1/1) blend or a 1,3,5-triallyl-1,3,5-triazine-2,4,6(1*H*,3*H*,5*H*)-trione (Trione)/Trithiol (1/1) blend (see Figure 8) [246]. Morin is a natural compound that can be extracted from Osage orange and is well known to exert antioxidant, anti-inflammatory and anti-carcinogenic effects [247–250].

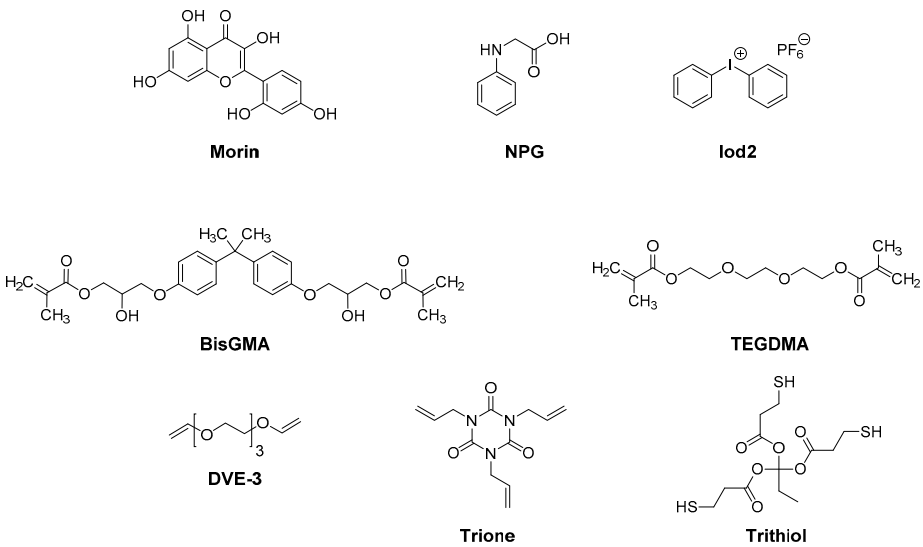

Figure 8. Chemical structure of quercetin and its isomer of position morin, different monomers and additives.

From the absorption viewpoint and despite the similarity of structures between quercetin and morin, totally different absorption spectra were determined in ethanol. If no absorption peaks could be detected for morin, an absorption peak could be clearly detected for quercetin (λ_{max} = 372 nm, ε = 23,300 M^{-1}·cm^{-1}) (see Figure 9). In addition, the absorption spectrum of morin extends up to 575 nm so that polymerization experiments could be carried out at 374, 394, 410 and 445 nm (see Table 1).

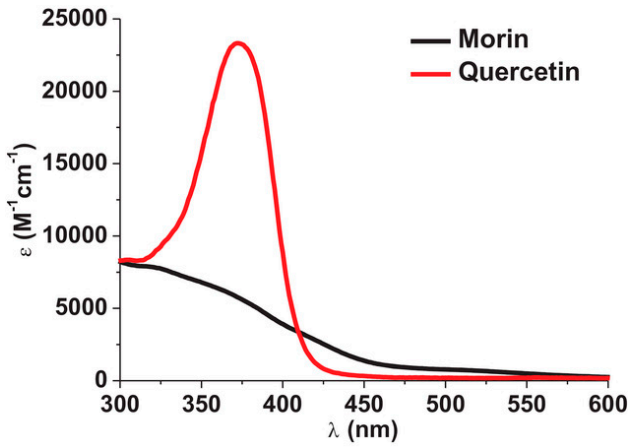

Figure 9. UV-visible absorption spectra of morin and quercetin in ethanol. Reproduced with permission from Ref. [246]. Copyright 2021, Wiley.

Table 1. Absorption properties of morin and quercetin in ethanol at different wavelengths.

	λ_{max} (nm)	ε_{max} ($M^{-1}\cdot cm^{-1}$)	ε_{374nm} ($M^{-1}\cdot cm^{-1}$)	ε_{394nm} ($M^{-1}\cdot cm^{-1}$)	ε_{410nm} ($M^{-1}\cdot cm^{-1}$)	ε_{445nm} ($M^{-1}\cdot cm^{-1}$)
morin	-	-	5700	4300	3360	1560
quercetin	372	23,300	23,200	13,960	3260	360

FRP experiments performed with morin and quercetin revealed the two-component morin/Iod2 system to be unable to initiate the FRP of the BisGMA/TEGDMA (70/30 *w*/*w*) blend upon irradiation at 410 and 445 nm. Conversely, a conversion of 26% was obtained with the quercetin/Iod2 system upon excitation at 410 nm (I = 110 mW/cm^2) for 300 s. No polymerization was detected at 445 nm with quercetin due to the lack of absorption. A significant improvement in the monomer conversion was obtained by using the three-component quercetin/Iod2/*N*-phenylglycine (NPG) (0.5%/2%/2% *w*/*w*/*w*) system. A conversion of 60% at 410 nm and 57% at 445 nm. These values are higher than those obtained with the reference NPG/Iod2 system (26% at 410 nm, 47% at 445 nm). While examining the cationic polymerization (CP) of DVE-3, the best monomer conversion was obtained at 410 nm with the two-component quercetin/Iod2 (0.5%/2% *w*/*w*) system (89% after 300 s of irradiation) vs. 78% with the morin/Iod2 system. Parallel to this, an induction time of 25 s was determined with the quercetin-based system contrarily to 110 s with morin. Finally, the two-component quercetin/Iod2 (0.5%/2%, *w*/*w*) system was examined for the thiol-ene polymerization of the DVE-3/Trithiol (1/1) and Trione/Trithiol (1/1) blends (see Figure 10).

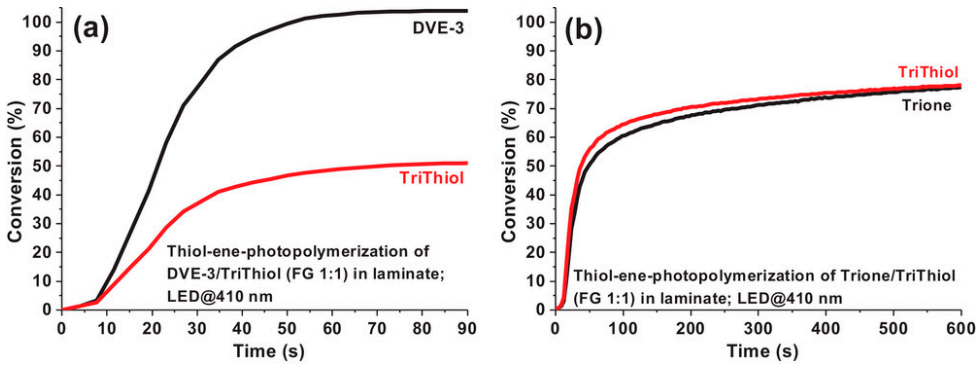

Figure 10. Thiol-ene polymerization of a DVE-3/Trithiol (1/1) blend (**a**) and a Trione/Trithiol (1/1) blend (**b**) upon irradiation at 410 nm. Reproduced with permission from Ref. [246]. Copyright 2021, Wiley.

Interestingly, DVE-3 was entirely polymerized in the presence of Trithiol for which a trithiol conversion of only 51% was detected. A shorter induction time was determined for DVE-3, reduced to only 8 s contrarily to 25 s for the homopolymerization of DVE-3. By replacing DVE-3 with Trione, a similar conversion was obtained for Trione and Trithiol, around 80% for the two monomers (see Figure 10b). To support the unequal monomer conversion determined during the thiol-ene polymerization of a DVE-3/Trithiol blend, the occurrence of a homopolymerization of DVE-3 concomitant to the thiol-ene polymerization was suggested. Conversely, homopolymerization of Trione is difficult, avoiding this undesired reaction [251–253].

In 2018, another flavonol, i.e., 3-hydroxyflavone (3HF) was used in combination with an amino acid, namely *N*-phenylglycine (NPG), to produce free radicals upon irradiation at 385, 405 and 477 nm (see Figure 11) [254].

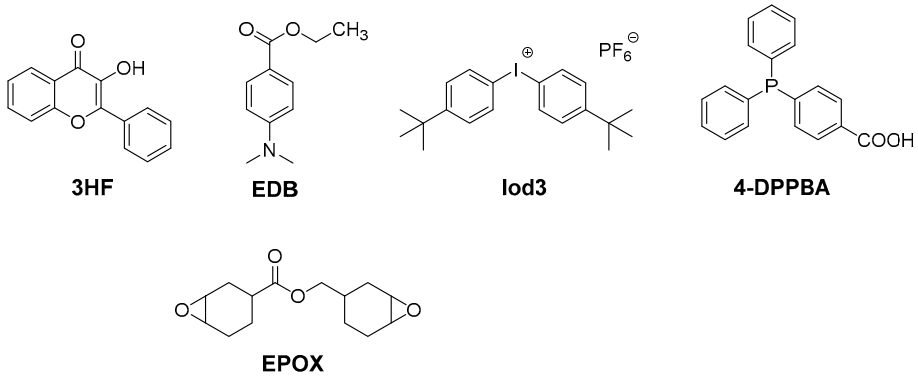

Figure 11. Chemical structures of 3HF, different monomers and additives.

From the absorption viewpoint, the absorption maximum of 3HF was blue-shifted by ca. 20 nm compared to quercetin (350 nm vs. 370 nm for 3HF). Only low molar extinction coefficients could be determined in the visible range, ranging between $\varepsilon \sim 250\ M^{-1}\cdot cm^{-1}$ at 405 nm and $\varepsilon \sim 40\ M^{-1}\cdot cm^{-1}$ at 470 nm. Conversely, at 350 nm, a molar extinction coefficient of ε~14,000 $M^{-1}\cdot cm^{-1}$ could be calculated. The high reactivity of 3HF was evidenced when combined with NPG. Thus, using the 3HF/NPG (0.5%/1% *w*/*w*) couple, a conversion as high as 71% could be determined during the FRP of a BisGMA/TEGDMA (1/1) blend (where BisGMA and TEGDMA stand for bisphenol A-glycidyl methacrylate and triethylene glycol dimethacrylate, respectively) (see Table 2) upon irradiation at 405 nm with an LED (I = 110 mW/cm^2).

Table 2. Monomer conversions obtained during the FRP and CP experiments using different photoinitiating systems.

Resin/PIS	Conditions	Conversion (%) at 100 s	Light Source
BisGMA/TEGDMA	3HF/Iod3 (0.5%/1% *w*/*w*)	19	LED@405 nm
	3HF/NPG (0.5%/1% *w*/*w*)	71	LED@405 nm
	3HF/NPG (0.5%/1% *w*/*w*)	48	LED@477 nm
	3HF/Iod3/NPG (0.5%/1%/1% *w*/*w*/*w*)	79	LED@405 nm
	3HF/Iod3/NPG (0.5%/1%/1% *w*/*w*/*w*)	65	LED@477 nm
	3HF/Iod3/EDB (0.5%/1%/1% *w*/*w*/*w*)	17	LED@385 nm
EPOX	3HF/Iod3/EDB (0.5%/1%/1% *w*/*w*/*w*)	55	LED@385 nm

This value is higher than that obtained with the reference Iod3/EDB (1%/1% *w*/*w*) system (68% after 100 s of irradiation at 405 nm) [255]. If an excellent monomer conversion could be obtained with the reductive pathway, a different situation was found using the oxidative one. Thus, only a low monomer conversion of 19% was obtained with the

two-component 3HF/Iod3 (0.5%/1% *w*/*w*) system upon irradiation at 405 nm. By using the three-component 3HF/Iod3/NPG (0.5%/1%/1% *w*/*w*/*w*) system, high monomer conversions could be determined at 405 and 477 nm (79 and 65%, respectively). In particular, the monomer conversion of 65% obtained at 477 nm is remarkable, considering the weak molar extinction coefficient of 3HF at 477 nm. The crucial role of the amine in the monomer conversion was evidenced by replacing NPG with ethyl 4-(dimethylamino)benzoate (EDB). In this case, the conversion was reduced to only 17%. The difference in reactivity for the three-component system based on EDB and NPG can be ascribed to the decarboxylation reaction occurring with NPG, avoiding back electron transfer [256,257]. Upon irradiation at 385 nm, the CP of EPOX furnished the high conversion of 55% after 100 s of irradiation with the three-component 3HF/Iod3/EDB (0.5%/1%/1% *w*/*w*/*w*) system. For comparison, only an EPOX conversion of 15% was obtained with the reference BAPO/Iod3 (0.5%/1% *w*/*w*) system in the same conditions. Considering the high performance of the different photoinitiating systems designed with 3HF as a photosensitizer, interest in these photoinitiating systems was demonstrated during direct laser writing experiments (see Figure 12) and during the design of composites (see Figure 13). In the case of the direct laser writing experiments, 3D patterns exhibiting an excellent spatial resolution could be evidenced.

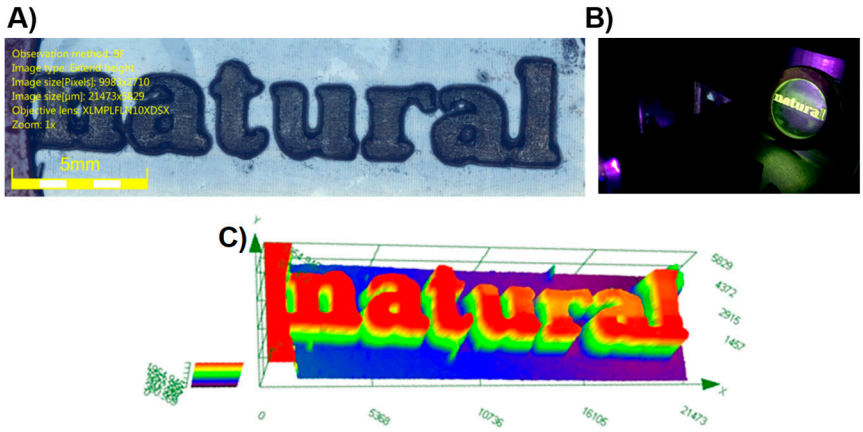

Figure 12. Direct laser writing experiments performed at 405 nm using a BisGMA/TEGDMA (70%/30%) blend as the monomer and the two-component 3HF/NPG (0.5%/1% *w*/*w*) system. (**A**) Logo. (**B**) Fluorescence of the 3D patterns. (**C**) Characterization of the 3D pattern by numerical optical microscopy. Reproduced with permission from Ref. [254]. Copyright 2018, The American Chemical Society.

Figure 13. FRP experiments of a BisGMA/TEGDMA (70%/30%) blend for composites cured using an LED emitting at 395 nm. Reprinted/adapted with permission from Ref. [254]. Copyright 2018, The American Chemical Society.

Composites were obtained by impregnating a BisGMA/TEGDMA (70%/30%) resin with glass fibers (50% glass fiber/50% resin). Using the 3HF/NPG combination, composites could be fully cured in only one pass (2 m/min belt speed) upon irradiation with an LED emitting at 395 nm.

To support the high efficiency of the 3HF/NPG and 3HF/Iod3 systems, the following mechanisms could be determined by combining steady-state photolysis and fluorescence quenching experiments, ESR and electrochemistry (see Equations (r6)–(r12)).

$$3HF \rightarrow {}^{1,3}3HF\ (h\nu) \tag{r6}$$

$${}^{1,3}3HF + NPG \rightarrow (3HF\text{-}H)^{\bullet} + NPG_{(-H)}{}^{\bullet} \tag{r7}$$

$$NPG_{(-H)}{}^{\bullet} \rightarrow NPG_{(-H;-CO2)}{}^{\bullet} \tag{r8}$$

$${}^{1,3}3HF + Iod \rightarrow 3HF^{\bullet+} + Ar_2I^{\bullet} \rightarrow Ar^{\bullet} \tag{r9}$$

$$NPG + Iod \leftrightarrow [NPG\text{-}\ Iod]_{CTC} \tag{r10}$$

$$[NPG\text{-}\ Iod]_{CTC} \rightarrow\rightarrow\rightarrow Ar^{\bullet}\ (h\nu) \tag{r11}$$

$$NPG_{(-H;-CO2)}{}^{\bullet} + Ar_2I^{+} \rightarrow NPG_{(-H;-CO2)}{}^{+} + Ar^{\bullet} + ArI \tag{r12}$$

In 2020, 3HF was revisited by Wang and coworkers in a series of seven flavonols differing in the substitution pattern (see Figure 14) [258]. The influence of halogens on the photoinitiating ability of flavonols could be examined, these groups being introduced at different positions on the flavonol core.

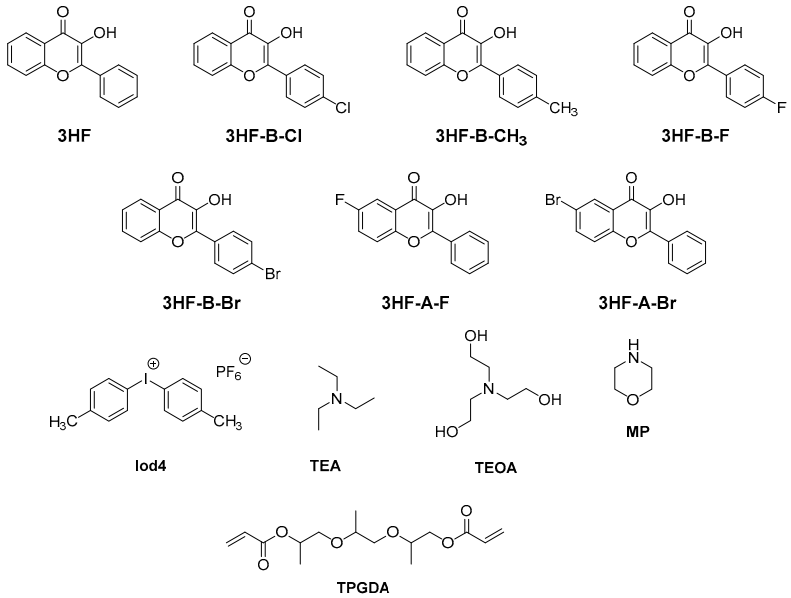

Figure 14. Chemical structures of different derivatives of 3HF, the monomer and different additives.

Noticeably, the absorption of the different dyes was not significantly affected by the halogen substitution, and absorption in the 280–450 nm range could be determined for all dyes. Thus, absorption maxima between 342 nm for 3HF and 3HF-B-F and 349 nm for 3HF-A-F were determined in methanol (see Figure 15 and Table 3). Examination of the fluorescence properties of the different 3HF revealed the presence of two emission peaks, the first one at ca. 450 nm, corresponding to the Franck–Condon excited state, and the second one at 550 nm, corresponding to the emission of the tautomer formed by ESIPT. In the case of 3HF-A-F and 3HF-A-Br, emission peaks at 450 nm could not be detected for these tow dyes, attributable to a fast ESIPT process.

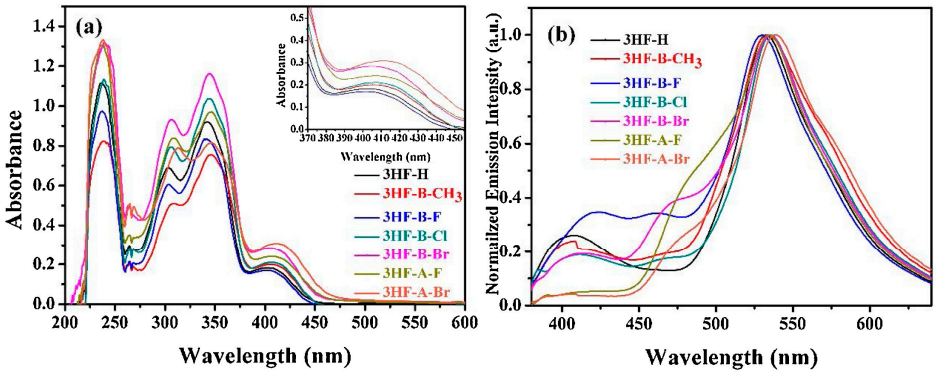

Figure 15. UV-visible absorption spectra (**a**) and fluorescence spectra (**b**) of different 3HF derivatives in methanol. Reproduced with permission from Ref. [258]. Copyright 2020, Elsevier.

Table 3. Optical characteristics of different 3HF derivatives in methanol.

3HF	λ_{max} (nm)	ε_{max} ($M^{-1}\cdot cm^{-1}$)	$\varepsilon_{385\ nm}$ ($M^{-1}\cdot cm^{-1}$)
3HF-H	342	17,800	1900
3HF-B-CH_3	347	14,700	2600
3HF-B-F	342	16,200	1850
3HF-B-Cl	345	19,900	2100
3HF-B-Br	346	20,500	2250
3HF-A-F	347	16,900	2400
3HF-A-Br	349	13,800	3200

Based on their absorption spectra, photopolymerization experiments were carried out at 385 nm. Photolysis experiments performed at 385 nm for the two-component dye/triethanolamine (TEOA) and dye/Iod4 systems revealed the photolysis rate to be higher for the two-component dye/Iod4 systems. The different dyes are thus easier to oxidize than to reduce. Fluorescence quenching experiments performed in methanol revealed the fluorescence of the ESIPT tautomer to be drastically reduced by increasing the concentration of Iod4 and TEOA, evidencing the reaction with the additives to be faster than the ESIPT process. In the case of the two-component dye/Iod4 systems, the formation of three different 3HF-based toluene adducts resulting from the addition of the toluene radical (formed by photoinduced electron transfer between the excited dye and the iodonium salt) to the 3HF dyes was detected by mass spectrometry.

Photopolymerization experiments were carried out on a difunctional monomer, namely tripropylene glycol diacrylate (TPGDA). Among the four amines tested for the two-component dye/amine systems (TEOA, morpholine (MP), triethylamine (TEA) and NPG) and irrespective of the 3HF derivatives examined, the highest monomer conversions were obtained with TEOA, whereas the lowest conversions were determined with NPG. Using TEOA as the amine, the influence of the substitution pattern on the photoinitiating ability could be examined. Thus, it was found that the introduction of halogens on the pendant phenyl ring was favorable for monomer conversions compared to the flavonol core. As shown in Figure 16b, higher monomer conversions were obtained with 3HF-B-F and 3HF-B-Br compared to their 3HF-A-F and 3HF-A-Br analogs. Except for 3HF-B-CH_3 and 3HF-A-Br, which furnished monomer conversions around 70% after 180 s of irradiation, all the other dyes furnished similar monomer conversions, peaking at 80%. While examining the series of flavonols substituted with different groups on the pendant phenyl ring, the introduction of electron-donating groups (such as 3HF-B-CH_3) reduced the monomer conversion and the polymerization rate, whereas the introduction of electron-withdrawing groups improved both the conversion and the polymerization rates. A different trend was found for the

dye/Iod3 system. Using the dye/Iod4 (0.2%/1% w/w) system, the highest polymerization rate was obtained with 3HF-B-CH_3, followed by 3HF-B-Cl, 3HF-B-Br, 3HF-B-F and 3HF. If different polymerization rates were determined using Iod4 as the co-initiator, similar conversions were obtained after 120 s of irradiation at 385 nm. A comparison with identical halogen atoms revealed the brominated derivatives to be more reactive than the fluorinated ones, and this trend of reactivity is comparable to that determined with the two-component dye/TEOA systems.

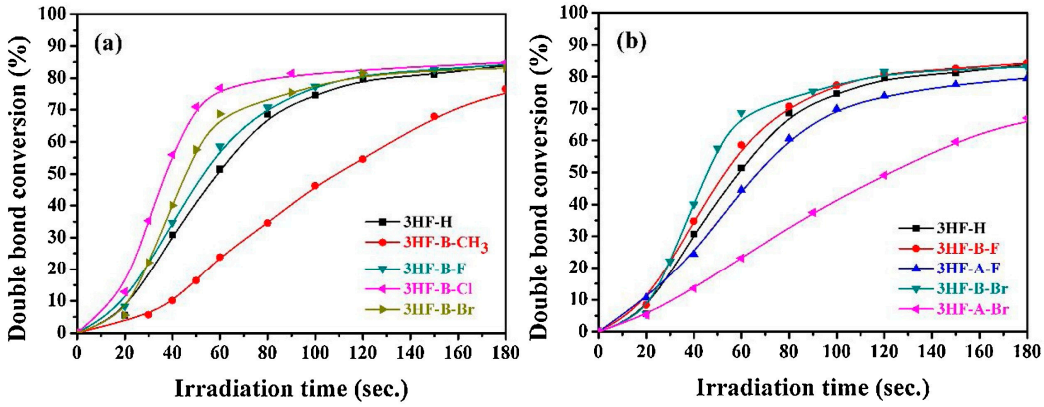

Figure 16. TPGDA conversions determined upon irradiation at 385 nm with an LED and by using the two-component dye/TEOA (1%/3% w/w) systems (**a**) first series of dyes (**b**) second series of dyes. Reproduced with permission from Ref. [258]. Copyright 2020, Elsevier.

In 2021, the same group developed an innovative strategy for the design of photoinitiating systems based on flavonols. Considering that the presence of the OH group is responsible for the ESIPT process which is a competitive process to photoinitiation, this intramolecular proton transfer could be efficiently avoided by etherifying or esterifying the OH group with benzoyl or benzenesulfonyl groups [259]. Using this strategy, the ESIPT process could be suppressed, and the design of highly efficient Type I photoinitiators became possible (see Figure 17). In particular, the triplet lifetime could be increased, and a reduction in the fluorescence intensity was jointly observed, resulting in an improvement in the photopolymerization efficiency.

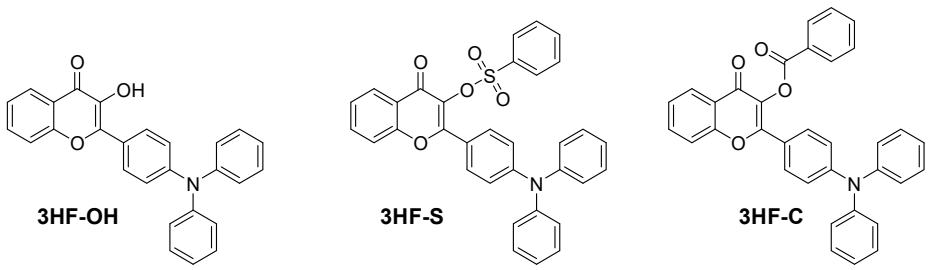

Figure 17. Chemical structures of flavonol-derived Type I photoinitiators.

Noticeably, 3HF-S and 3HF-C could act as efficient monocomponent systems during the FRP of TPGDA but also in combination with TEOA or Iod4 upon irradiation at 405 and at 460 nm with LEDs. Photopolymerization results also revealed the polymerization efficiency of 3HF-S to be higher than that of 3HF-C and 3HF-OH. In particular, the polymerization efficiency of 3HF-S could be greatly improved by decreasing the photoinitiator content, 3HF-S exhibiting aggregation-induced emission (AIE) properties adversely affecting its polymerization efficiency. From the absorption viewpoint, the presence of the triphenylamine moiety was the key element to redshift the absorption of 3HF-C, 3HF-S and 3HF-OH compared to those previously reported by Lalevée and coworkers [178]. Thus, absorption maxima located at 384, 386 and 396 nm were determined for 3HF-C, 3HF-S and

3HF-OH (see Figure 18). Interestingly, the broad absorption band extending up to 480 nm enabled the polymerization tests to be carried out at 405 nm but also at a longer wavelength, namely 460 nm. The solubility of photoinitiators is an important parameter governing the reactivity. Indeed, a low solubility in monomers will adversely affect the polymerization efficiency. As shown in Table 4, 3HF-S exhibited the highest solubility of the three dyes. In particular, compared to 3HF-OH, an improvement in the solubility was determined for the OH-substituted dyes, namely 3HF-C and 3HF-S. Among these dyes, 3HF-S showed the best solubility in aqueous solutions, favorable to polymerization processes used in green conditions. The photoacid generation abilities of 3HF–S and 3HF–C were also examined in acetonitrile using Rhodamine B as an acid indicator upon irradiation with an LED at 405 nm. Interestingly, 3HF-S exhibited the best photoacid generation ability (ϕ_{H+} = 0.2), significantly higher than that of 3HF-C for which a value of only 0.002 was determined. This is directly related to the fact that benzenesulfonic acid is generated with 3HF-S after photocleavage, contrary to benzoic acid in the case of 3HF-C.

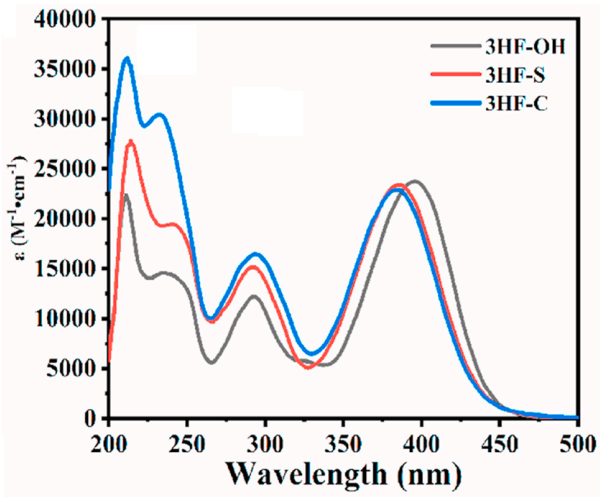

Figure 18. UV-visible absorption spectra of 3HF-OH, 3HF-C and 3HF-C in acetonitrile. Reproduced with permission from Ref. [259]. Copyright 2021, Elsevier.

Table 4. Solubility of different flavonols in various solvents at room temperature (g/100 mL).

	Toluene	Ethyl Acetate	THF	CH_3OH	CH_3CN	DMSO	CH_3OH:H_2O (1:1)	CH_3CN:H_2O (1:1)	DMSO:H_2O (1:1)
3HF-OH	0.9	2.0	2.0	1.4	0.8	3.5	0.5	0.7	0.7
3HF-S	8.0	5.0	>10	1.7	1.8	>10	0.8	1.0.	2.0
3HF-C	6.4	3.9	8.2	1.5	1.3	>10	0.6	0.8	1.6

FRP experiments of TPGDA performed at 405 and 460 nm revealed the photoinitiating ability of 3HF-C and 3HF-S to outperform that of the reference 3HF-OH. Using 3HF-S as a monocomponent system at 405 nm, a photoinitiator concentration as low as 0.125 wt% could be used while maintaining a high monomer conversion. Eighty-percent conversions could thus be obtained after 180 s of irradiation at 405 nm using 3HF-S. Conversely, no monomer conversion could be detected with 3HF-OH when used as a monocomponent system. The use of 3HF-S in a two-component system enabled drastic shortening of the reaction time using additives such as triethanolamine (TEOA) or triethylamine (TEA) as the amines. By using TEA and TOEA, 80% conversions could be obtained within 20 s. A threefold elongation of the reaction time was determined by using MP and EDB as the amines. Finally, by using NPG as the additive for 3HF-S, 180 s were required to get 80% TPGDA conversion (see Figure 19). Comparisons of the TPGDA conversions obtained with camphorquinone (CQ) in one- and two-component systems revealed the 3HF-S-based

systems to outperform those prepared with camphorquinone, irrespective of the irradiation wavelength (405 nm or 460 nm). 3HFs were also used for the sensitization of Iod4 (see Figure 20). In this case, short reaction times (i.e., 20 s) were determined with all systems, evidencing that 3HFs were easier to oxidize than to reduce. Conversions ranging between 85 and 90% could be obtained within 30 s.

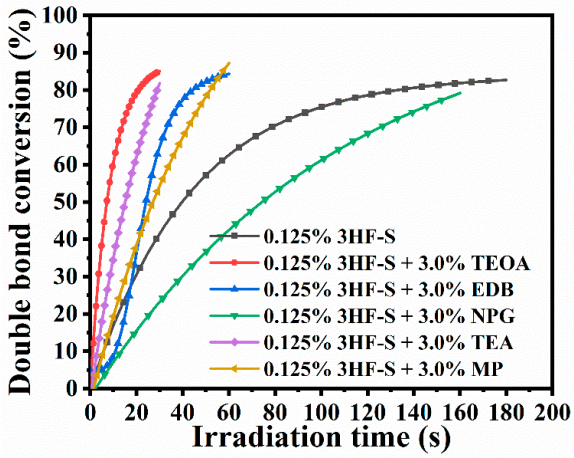

Figure 19. Photopolymerization profiles of TPGDA at 405 nm using an LED and 3HF-S (0.125% wt), 3HF-S/TEOA (0.125%/3.0% *w*/*w*); 3HF-S/EDB (0.125%/3.0% *w*/*w*); 3HF-S/NPG (0.125%/3.0% *w*/*w*); 3HF-S/TEA (0.125%/3.0% *w*/*w*) and 3HF-S/MP (0.125%/3.0% *w*/*w*). Reproduced with permission from Ref. [259]. Copyright 2021, Elsevier.

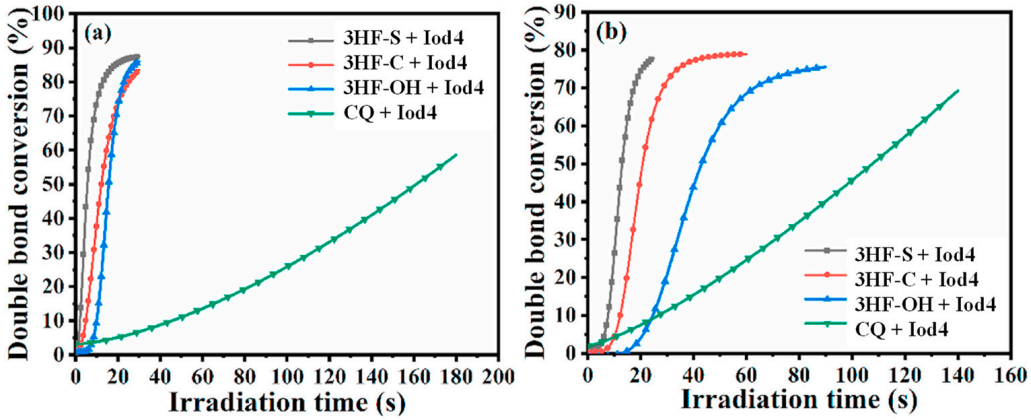

Figure 20. Photopolymerization profiles of TPGDA at 405 nm (**a**) and 460 nm (**b**) using 3HFs/Iod4 (0.125%/1.0% *w*/*w*) and CQ/Iod4 (0.125%/1.0% *w*/*w*). Reprinted/adapted with permission from Ref. [259]. Copyright 2021, Elsevier.

Considering the good solubility of 3HF-S in water, the polymerization of hydrogels could be performed at 405 nm. Using PEGDA (70% in water), an excellent monomer conversion could be determined by using a photoinitiator content as low as 0.042 wt%. After 60 s of irradiation at 405 nm, final conversions of 33, 75 and 85% were determined by using 3HF–S (0.042 wt%), 3HF-S/TEOA (0.042%/3% *w*/*w*) and 3HF-S/Iod4 (0.042%/3% *w*/*w*), respectively (see Figure 21).

By ESR spin-trapping experiments, the photochemical mechanism involved with the one- and two-component systems could be determined, and the results are summarized in Scheme 1.

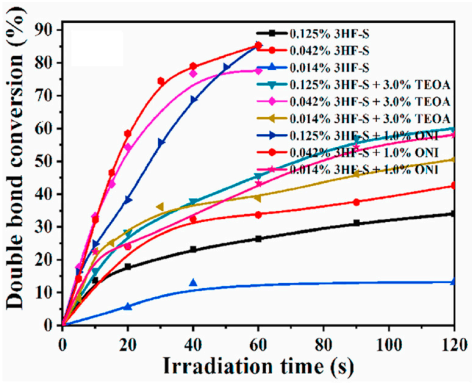

Figure 21. Polymerization profiles determined at 405 nm using different one- and two-component systems based on 3HF-S. (Note: Iod4 corresponds to ONI in the Figure.) Reproduced with permission from Ref. [259]. Copyright 2021, Elsevier.

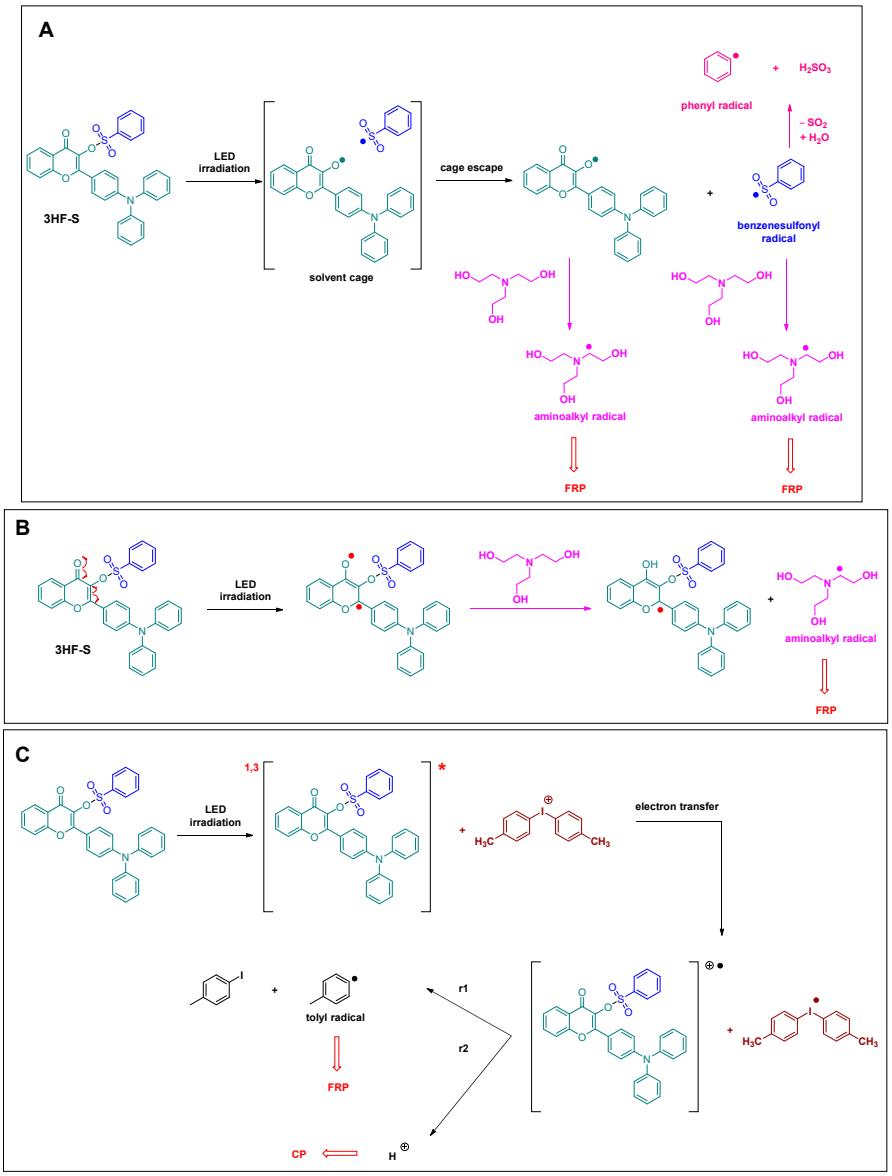

Scheme 1. Photochemical mechanism involved with the different one- and two-component systems (**A**) and (**B**) The two possible mechanism of reaction of 3HF-S with TEOA and (**C**) reaction of 3HF-S with an iodonium salt.

Examination of the cytotoxicity of the polymer films prepared with CQ, 3HF-S and 3HF-C revealed the cell viability of HeLa cells to be higher than 80%, whereas cell viability lower than 80% was determined for polymers prepared with 3HF-OH. Considering that sulfonate derivatives can outperform all other derivatives, another sulfonate derivative, i.e., 3HF-F, was examined, bearing a pendant carbazoyl group (see Figure 22) [260]. Using this high-performance photoinitiator in three-component 3HF-F/Iod4/TEOA (0.5%/2%/1% *w*/*w*/*w*) systems, 4D-printed objects could be designed and synthesized. As shown in Figure 23, the presence of the carbazoyl moiety was crucial in order to get a significant absorption in the visible range. Indeed, the reference compound, namely 3HF-A, bearing a tolyl group, only exhibited UV-centered absorption, evidencing the role of the carbazole moiety in the absorption properties. In particular, 4D-printed objects could be prepared using a hydrophilic monomer, namely PEGDA, enabling the use of a sequence of hydration/dehydration for designing shape memory objects (snowflake and airplane) (see Figure 24).

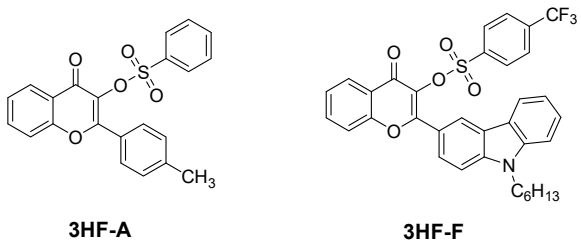

Figure 22. Chemical structures of 3HF-A and 3HF-F.

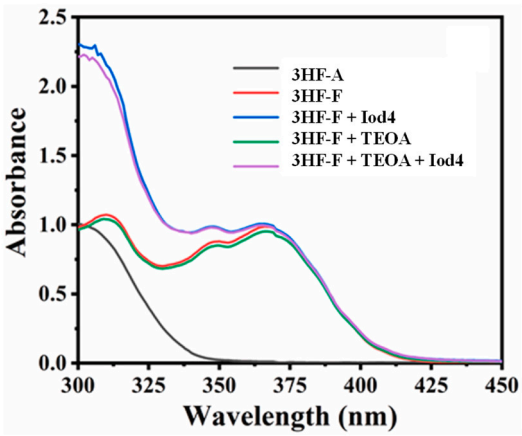

Figure 23. UV-visible absorption of 3HF-A and 3HF-F in acetonitrile. Reproduced with permission from Ref. [260]. Copyright 2022, Elsevier.

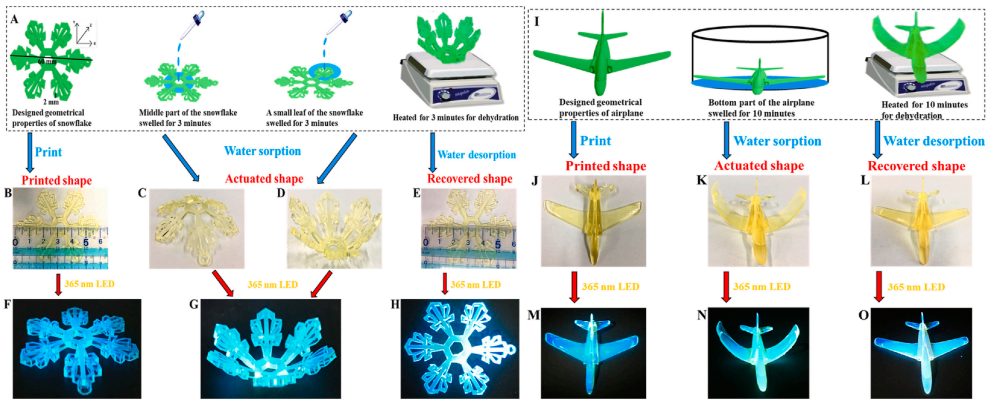

Figure 24. The different steps involved in the shape modification of 3D-printed objects ((**A**–**H**): snowflake, (**I**–**O**): airplane). Reproduced with permission from Ref. [260]. Copyright 2022, Elsevier.

It has to be noticed that this strategy (hydration/dehydration) has been extensively used by Lalevée and coworkers for designing 4D-printed objects by using chalcones as the chromophores [9,127,261,262].

In 2023, an interesting strategy was developed for the design of Type I photoinitiators, consisting in introducing a camphorquinone derivative on the photocleavable side [263]. Five derivatives were investigated, differing by the substitution of the flavonol core (see Figure 25).

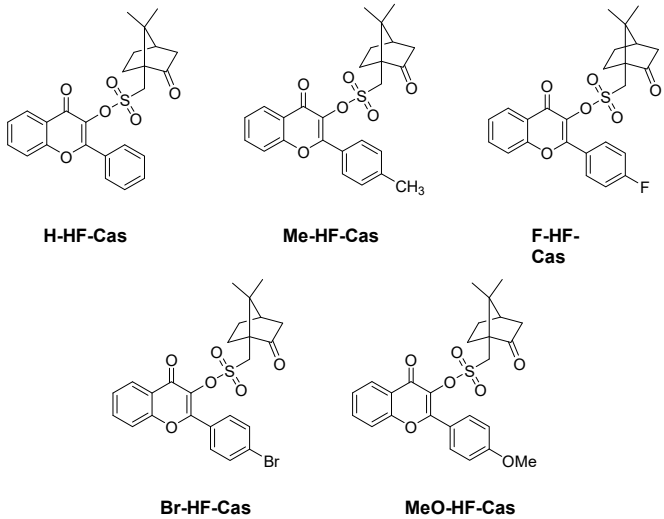

Figure 25. Chemical structures of Type I photoinitiators based on camphorsulfonate.

The choice of camphorsulfonic acid as the additional chromophore was motivated by the different advantages this photoinitiator exhibits such as low sensitivity to oxygen, good water solubility and low toxicity [264,265]. From the absorption viewpoint, almost similar absorption maxima were determined for the different dyes, except for MeO-HF-Cas bearing an electron donating group and for which a redshifted absorption was determined. Thus, absorption maxima located at 294, 295, 296, 300 and 313 nm were respectively determined for H-HF-Cas, F-HF-Cas, Br-HF-Cas, Me-HF-Cas and MeO-HF-Cas (see Figure 26 and Table 5).

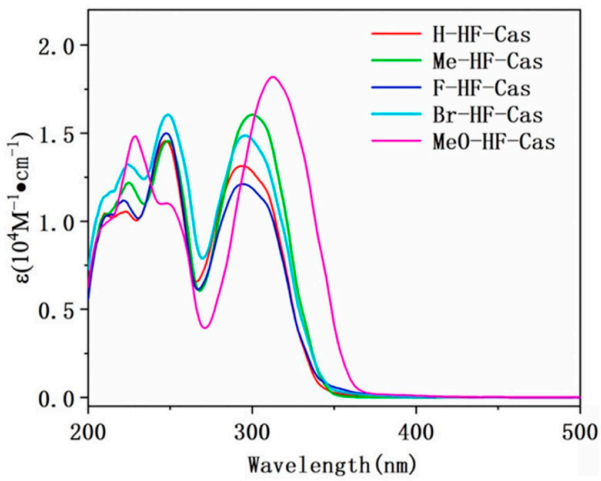

Figure 26. UV-visible absorption spectra of dyes in acetonitrile. Reproduced with permission from Ref. [263]. Copyright 2023, MDPI.

Table 5. Optical characteristics of different flavonol camphorsulfonates and quantum yield of photoacid generation in acetonitrile.

Compounds	λ_{max} (nm)	ε_{max} ($M^{-1}\cdot cm^{-1}$)	$\varepsilon_{365\ nm}$ ($M^{-1}\cdot cm^{-1}$)	λ_{em1} (nm)	λ_{em1} (nm)	Stokes Shift (cm^{-1})	$\Phi_{(H+)}$ [a]
H-HF-Cas	294	13,150	106	378	531	5235	0.06
Me-HF-Cas	300	16,000	34	381	530	5347	0.31
F-HF-Cas	295	12,100	285	377	528	5319	0.22
Br-HF-Cas	296	14,850	189	382	535	5154	0.39
MeO-HF-Cas	313	18,200	395	396	532	5494	0.29

[a] quantum efficiency of photoacid generation.

Examination of their fluorescence properties also revealed that the different dyes exhibit a dual emission, with an emission in the UV range and a second one in the visible range. Even if the ESIPT effect is hindered by the substitution of the OH group at the C_3-position, the intramolecular charge transfer still exists, with the presence of tautomers in the excited state, as shown in Scheme 2. Considering the similarity of emission around 530 nm, the low contribution of the aromatic ring on the fluorescence de-excitation process was determined.

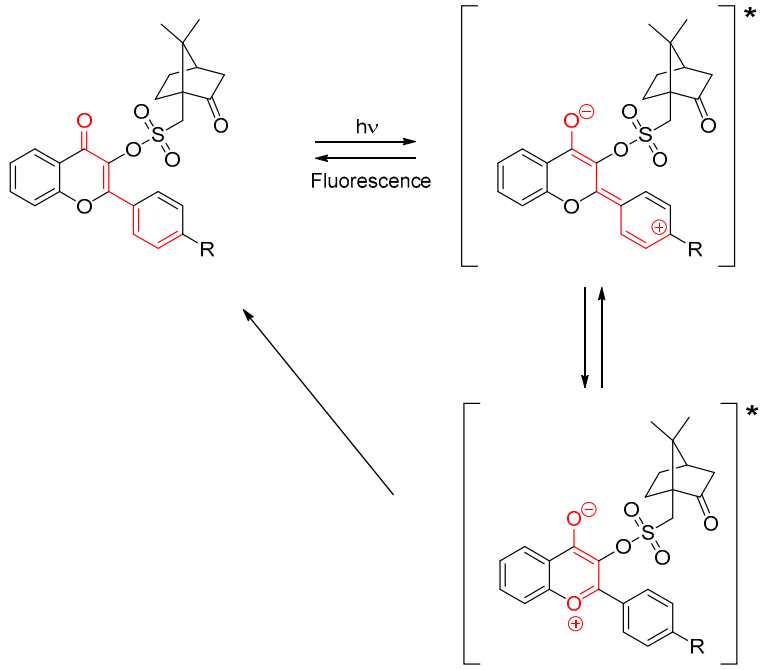

Scheme 2. Rearrangement of flavonol camphorsulfonates in the excited state (*).

Photolysis experiments performed in acetonitrile confirmed the Type I behavior of the different flavonol camphorsulfonates. Upon irradiation at 365 nm, photocleavage of flavonols can clearly be evidenced by NMR. Investigation of the photolysis products by mass spectrometry enabled us to confirm the formation of camphorsulfonic acid and the corresponding flavonol due to water traces in acetonitrile (see Scheme 3). Flavonol camphorsulfonates can thus behave as photoacid generators [266].

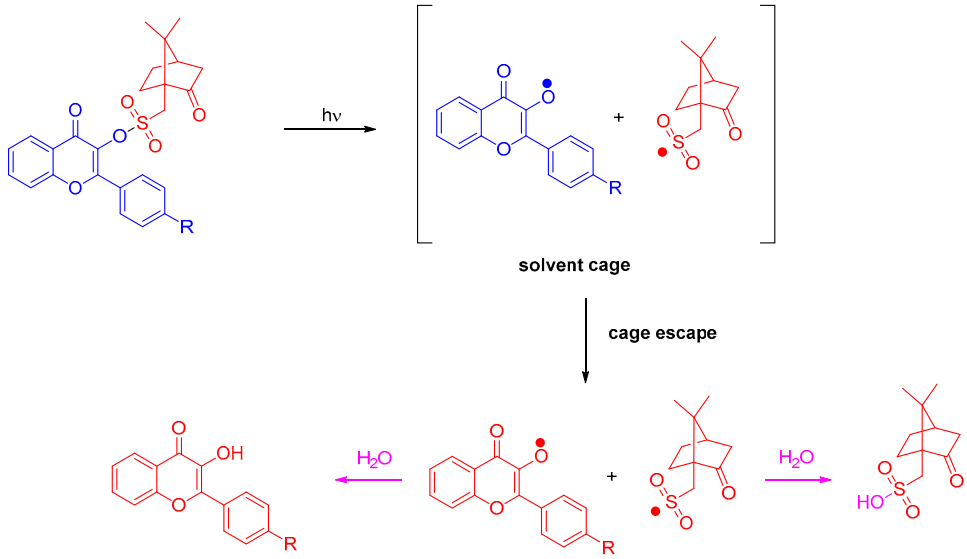

Scheme 3. Mechanism of photolysis of flavonol camphorsulfonates.

The highest photoacid generation quantum yield was determined for Br-HF-Cas bearing a halogen atom upon excitation at 365 nm (see Table 5). In this context, the cationic polymerization of DVE-3 was examined with the different photoinitiators. Upon excitation at 365 nm, only low monomer conversions were obtained using a 1 wt% photoinitiator, consistent with the low photoacid generation ability of camphorsulfonic acid and the inability of the flavonol moiety to initiate a cationic polymerization process. By using flavonol camphorsulfonates as monocomponent systems (1 wt%), the free radical polymerization of PEGDA could be efficiently initiated, and conversions of 80, 96, 91, 88 and 67% were respectively obtained with Me-HF-Cas, F-HF-Cas, Br-HF-Cas, MeO-HF-Cas and H-HF-Cas. By using the different flavonol camphorsulfonates as photosensitizers for Iod4, a slight improvement in the PEGDA conversion could be detected with the two-component dye/Iod4 (0.1%/0.1% *w*/*w*) systems. Thus, PEGDA conversions of 90, 84, 86 and 85% could be obtained after 120 s of irradiation at 365 nm using MeO-HF-Cas, Me-HF-Cas, Br-HF-Cas, F-HF-Cas and Me-HF-Cas.

2.2. Flavones

Flavonoids are composed of a large group of polyphenolic dyes, and flavone is one of them. Flavone was used as early as 2016 for the photoinduced controlled/"living" polymerization of MMA [267]. Using an LED emitting in the 350–440 nm range, linear PMMA polymers with a polydispersity index (PDI) ranging between 1.34 and 1.42 could be prepared by photopolymerization. Even if the approach is promising, the control of the polymerization process is still lower than what can be currently obtained by thermal polymerization. Photopolymerization is more classically used for the polymerization of multifunctional monomers, and this point was only recently examined by Lalevée and coworkers for the FRP of a dental resin, i.e., a BisGMA/TEGDMA 70/30 blend (see Figure 27) [268]. Different flavones were investigated in this work, all these derivatives being natural products. Notably, chrysin can be found in the flowers of blue passionflower (Passiflora caerulea) and myricetin in various edible plants such as onion leaves, Semambu leaves, bird chili, black tea, papaya shoots and guava [269–276]. As specificities, these dyes are also (poly)phenolic dyes, and phenols are extensively used as stabilizers for monomers [277,278]. In addition, efficient polymerization processes could be performed with these structures.

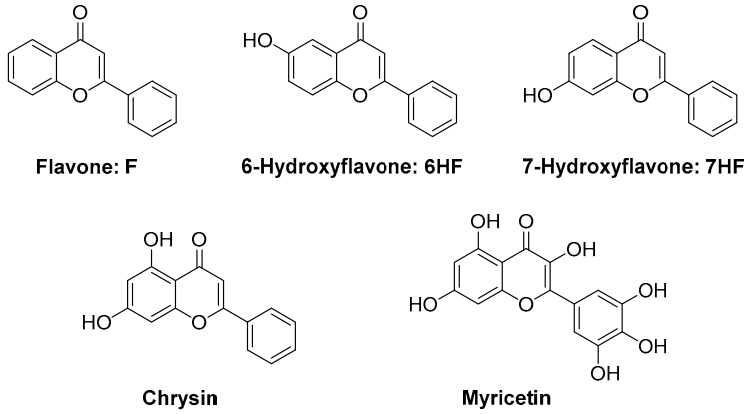

Figure 27. Chemical structures of different flavones used as photoinitiators of polymerization.

As shown in Figure 28, all dyes exhibit UV-centered absorption, except for myricetin for which a redshift of the absorption was detected for this dye. It can be assigned to the presence of the numerous OH groups acting as electron-withdrawing groups, improving the electronic delocalization existing in this structure. An absorption extending up to 450 nm could be determined for Myricetin, whereas almost no absorption could be detected anymore for the other dyes. The efficiency of the polymerization process is also strongly related to the solubility of the photosensitizers in resins. This point was notably examined in TMPTA and BisGMA/TEGDMA. Noticeably, the increase in the OH groups per dye adversely affected the solubility of dyes. Thus, the worse solubilities were determined for Chrysin and Myricetin (see Table 6).

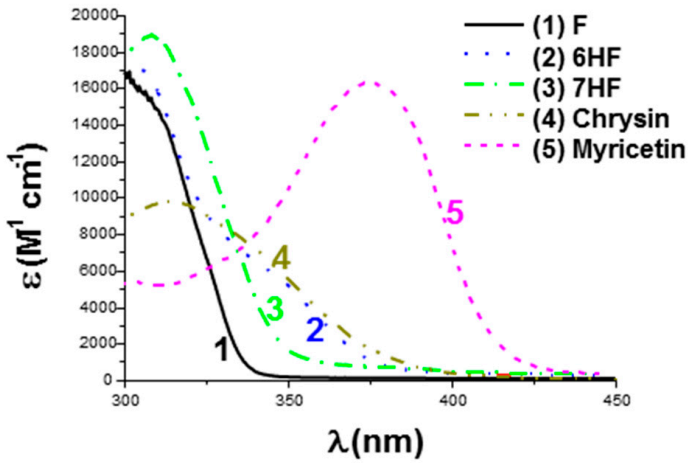

Figure 28. UV-visible absorption spectra of dyes in methanol. Reproduced with permission from Ref. [268]. Copyright 2020, Wiley.

Table 6. Absorption properties of dyes at 405 nm in methanol and monomers.

	F	6HF	7HF	Chrysin	Myricetin
Absorption properties at 405 nm ($M^{-1}\cdot cm^{-1}$) in methanol	~70	~70	~427	~336	4800
Solubility in BisGMA/TEGDMA	+	+	+	-	-
Solubility in TMPTA	+	+	+	-	-

Examination of their photoinitiating abilities during the FRP of TMPTA in thin films revealed the two-component dye/Iod3 system to be inefficient for promoting any polymerization. Conversely, by using the two-component dye/NPG system and the

three-component dye/Iod3/NPG system, a monomer conversion could be detected with the different dyes. Among them, 6HF furnished good monomer conversions both at 385 and 405 nm, as shown in Figure 29. The highest monomer conversion was obtained at 385 nm, using the three-component 6HF/Iod3/NPG (0.5%/1%/1% *w*/*w*/*w*) system, resulting from the perfect adequation between the emission of the LED and the absorption of the chromophore. At 405 nm, a reduction in the monomer conversion by ca. 10% could be determined, consistent with a decrease in the molar extinction coefficient. Noticeably, an important effect of the additives could be evidenced. Thus, by using EDB as the amine in three-component systems, a severe reduction in the monomer conversion could be determined, compared to that obtained with NPG. This was assigned to the strong oxygen inhibition competing with initiation [26,228,279–283]. This point was evidenced by using 4-dppba as the additive. Indeed, phosphines are well known to convert the unreactive peroxyl radicals as initiating alkoxyl radicals [279,284,285]. Using the three-component 6HF/Iod3/4-dppba (0.5%/1%/1% *w*/*w*/*w*) system at 385 nm, a conversion comparable to that obtained with the three-component 6HF/Iod3/NPG (0.5%/1%/1% *w*/*w*/*w*) system could be obtained.

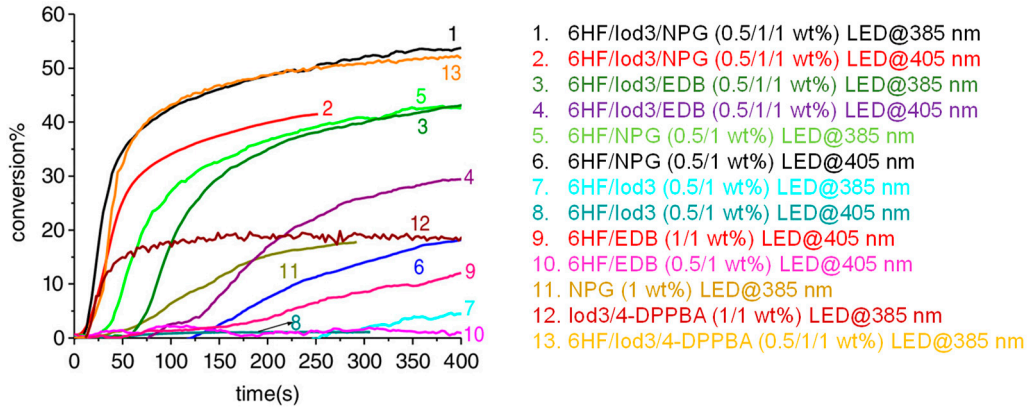

Figure 29. TMPTA conversions determined with different photoinitiating systems with 6HF as the photosensitizer both at 385 and 405 nm. Reproduced with permission from Ref. [268]. Copyright 2020, Wiley.

The high reactivity of the three-component 6HF/Iod3/NPG (0.5%/1%/1% *w*/*w*/*w*) system was confirmed during the FRP experiments performed on another resin, i.e., a BisGMA/TEGDMA blend. Surprisingly, if 3-hydroxyflavone 3HF previously studied proved to be an efficient photoinitiator for promoting the CP of EPOX at 385 nm, only a low monomer conversion could be obtained with the two-component 6-hydroxyflavone/Iod3 (0.5%/1% *w*/*w*) (40% conversion after 800 s of irradiation at 385 nm vs. 55% for the three-component 3HF/Iod3/EDB (0.5%/1%/1% *w*/*w*/*w*)) system, evidencing the strong influence of the substitution pattern on the overall reactivity of the photoinitiating system. In addition, the high monomer conversion obtained during the FRP of BisGMA/TEGDMA paves the way for dental applications of flavones [286].

2.3. Proanthocyanidins

Proanthocyanidins are flavonoids that can be found in black, red and purple rice, in other strongly colored fruits and vegetables and also in cereals such as blueberries, grapes, red cabbages and purple sweet potatoes [287–293]. Due to their high molar extinction coefficients, proanthocyanidins were thus ideal candidates for photopolymerization performed under visible light. In 2021, Wang and coworkers examined a series of proanthocyanidins substituted with methacrylate groups (see Figure 30) [294,295].

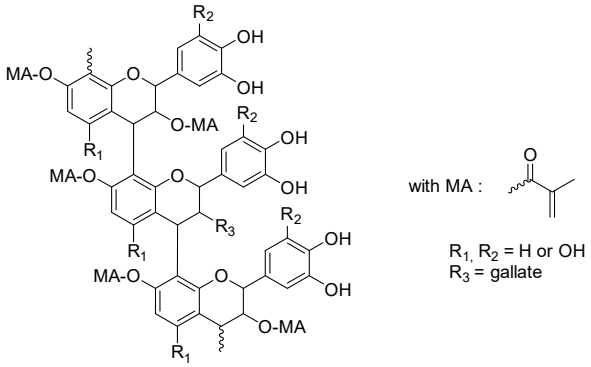

Figure 30. Chemical structures of methacrylate-based proanthocyanidins.

By the presence of methacrylate groups, polymerizable crosslinkers could be obtained, and the resulting polymers could be advantageously used for collagen stabilization in 2-hydroxyethylmethacrylate (HEMA)-based dental adhesive systems. In particular, an improvement in the longevity of the dental restoration could be evidenced by using these modified proanthocyanins.

3. Conclusions

Flavonoids are composed of numerous families of dyes, and only a few of them have been examined to date in photopolymerization. Even if more than 6000 flavonoids have been identified in nature, the scarcity of these structures renders their uses as photoinitiators of polymerization relatively improbable. In addition, for the most abundant ones, polymerization results obtained with these structures are remarkable, including excellent biocompatibility, the possibility to perform polymerization experiments at low photoinitiator content and the design of antibacterial coatings. At present, flavonoids could efficiently promote the FRP of acrylates or the CP of epoxides by the use of two- and three-component systems. To expend the scope of applications of flavonoids to photopolymerization, several points can be examined:

- At present, no monocomponent systems have been developed. In addition, by chemical modification, the covalent linkage of hydrogen donors or iodonium salts could contribute to simplifying the composition of the photocurable resins.
- Polymerization in water has only been scarcely examined.
- The design of Type I photoinitiators with the development of structures such as two oxime esters or glyoxylates should be explored.

Future works will consist of developing and exemplifying these different research topics.

Funding: This research received no external funding.

Conflicts of Interest: The author declares no conflict of interest.

References

1. Jasinski, F.; Zetterlund, P.B.; Braun, A.M.; Chemtob, A. Photopolymerization in Dispersed Systems. *Prog. Polym. Sci.* **2018**, *84*, 47–88. [CrossRef]
2. Noè, C.; Hakkarainen, M.; Sangermano, M. Cationic UV-Curing of Epoxidized Biobased Resins. *Polymers* **2021**, *13*, 89. [CrossRef] [PubMed]
3. Yuan, Y.; Li, C.; Zhang, R.; Liu, R.; Liu, J. Low Volume Shrinkage Photopolymerization System Using Hydrogen-Bond-Based Monomers. *Prog. Org. Coat.* **2019**, *137*, 105308. [CrossRef]
4. Khudyakov, I.V.; Legg, J.C.; Purvis, M.B.; Overton, B.J. Kinetics of Photopolymerization of Acrylates with Functionality of 1−6. *Ind. Eng. Chem. Res.* **1999**, *38*, 3353–3359. [CrossRef]
5. Dickens, S.H.; Stansbury, J.W.; Choi, K.M.; Floyd, C.J.E. Photopolymerization Kinetics of Methacrylate Dental Resins. *Macromolecules* **2003**, *36*, 6043–6053. [CrossRef]
6. Maffezzoli, A.; Pietra, A.D.; Rengo, S.; Nicolais, L.; Valletta, G. Photopolymerization of Dental Composite Matrices. *Biomaterials* **1994**, *15*, 1221–1228. [CrossRef] [PubMed]

7. Dikova, T.; Maximov, J.; Todorov, V.; Georgiev, G.; Panov, V. Optimization of Photopolymerization Process of Dental Composites. *Processes* **2021**, *9*, 779. [CrossRef]
8. Andreu, A.; Su, P.-C.; Kim, J.-H.; Ng, C.S.; Kim, S.; Kim, I.; Lee, J.; Noh, J.; Subramanian, A.S.; Yoon, Y.-J. 4D Printing Materials for Vat Photopolymerization. *Addit. Manuf.* **2021**, *44*, 102024. [CrossRef]
9. Chen, H.; Noirbent, G.; Zhang, Y.; Sun, K.; Liu, S.; Brunel, D.; Gigmes, D.; Graff, B.; Morlet-Savary, F.; Xiao, P.; et al. Photopolymerization and 3D/4D Applications Using Newly Developed Dyes: Search around the Natural Chalcone Scaffold in Photoinitiating Systems. *Dye. Pigment.* **2021**, *188*, 109213. [CrossRef]
10. Bagheri, A.; Jin, J. Photopolymerization in 3D Printing. *ACS Appl. Polym. Mater.* **2019**, *1*, 593–611. [CrossRef]
11. Fouassier, J.P.; Lalevée, J. Three-Component Photoinitiating Systems: Towards Innovative Tailor Made High Performance Combinations. *RSC Adv.* **2012**, *2*, 2621–2629. [CrossRef]
12. Lalevée, J.; Fouassier, J.-P. *Dyes and Chromophores in Polymer Science*; ISTE Ltd. and John Wiley & Sons Inc.: Hoboken, NJ, USA, 2015; ISBN 978-1-84821-742-3.
13. Tomal, W.; Kiliclar, H.C.; Fiedor, P.; Ortyl, J.; Yagci, Y. Visible Light Induced High Resolution and Swift 3D Printing System by Halogen Atom Transfer. *Macromol. Rapid Commun.* **2023**, *44*, 2200661. [CrossRef] [PubMed]
14. Gao, Y.; Lalevée, J.; Simon-Masseron, A. An Overview on 3D Printing of Structured Porous Materials and Their Applications. *Adv. Mater. Technol.* **2023**, *8*, 2300377. [CrossRef]
15. Liu, S.; Borjigin, T.; Schmitt, M.; Morlet-Savary, F.; Xiao, P.; Lalevée, J. High-Performance Photoinitiating Systems for LED-Induced Photopolymerization. *Polymers* **2023**, *15*, 342. [CrossRef] [PubMed]
16. Zeng, B.; Cai, Z.; Lalevée, J.; Yang, Q.; Lai, H.; Xiao, P.; Liu, J.; Xing, F. Cytotoxic and Cytocompatible Comparison among Seven Photoinitiators-Triggered Polymers in Different Tissue Cells. *Toxicol. Vitr.* **2021**, *72*, 105103. [CrossRef] [PubMed]
17. Ji, X.; Liang, J.; Liu, J.; Shen, J.; Li, Y.; Wang, Y.; Jing, C.; Mabury, S.A.; Liu, R. Occurrence, Fate, Human Exposure, and Toxicity of Commercial Photoinitiators. *Environ. Sci. Technol.* **2023**, *57*, 11704–11717. [CrossRef]
18. Xiong, Y.; Zou, H.; Wang, S.; Guo, J.; Zeng, B.; Xiao, P.; Liu, J.; Xing, F. Characteristics of a Novel Photoinitiator Aceanthrenequinone-Initiated Polymerization and Cytocompatibility of Its Triggered Polymer. *Toxicol. Rep.* **2022**, *9*, 191–203. [CrossRef]
19. Nguyen, A.K.; Goering, P.L.; Reipa, V.; Narayan, R.J. Toxicity and Photosensitizing Assessment of Gelatin Methacryloyl-Based Hydrogels Photoinitiated with Lithium Phenyl-2,4,6-Trimethylbenzoylphosphinate in Human Primary Renal Proximal Tubule Epithelial Cells. *Biointerphases* **2019**, *14*, 021007. [CrossRef]
20. Carve, M.; Wlodkowic, D. 3D-Printed Chips: Compatibility of Additive Manufacturing Photopolymeric Substrata with Biological Applications. *Micromachines* **2018**, *9*, 91. [CrossRef]
21. Bail, R.; Patel, A.; Yang, H.; Rogers, C.M.; Rose, F.R.A.J.; Segal, J.I.; Ratchev, S.M. The Effect of a Type I Photoinitiator on Cure Kinetics and Cell Toxicity in Projection-Microstereolithography. *Procedia CIRP* **2013**, *5*, 222–225. [CrossRef]
22. Tomal, W.; Ortyl, J. Water-Soluble Photoinitiators in Biomedical Applications. *Polymers* **2020**, *12*, 1073. [CrossRef] [PubMed]
23. Liu, R.; Mabury, S.A. First Detection of Photoinitiators and Metabolites in Human Sera from United States Donors. *Environ. Sci. Technol.* **2018**, *52*, 10089–10096. [CrossRef] [PubMed]
24. Wiesner, T.; Haas, M. Do Germanium-Based Photoinitiators Have Potential Replace Well-Establ. Acylphosphine Oxides? *Dalton Trans.* **2021**, *50*, 12392–12398. [CrossRef] [PubMed]
25. Ghazali, H.S.; Askari, E.; Seyfoori, A.; Naghib, S.M. A High-Absorbance Water-Soluble Photoinitiator Nanoparticle for Hydrogel 3D Printing: Synthesis, Characterization and In Vitro Cytotoxicity Study. *Sci. Rep.* **2023**, *13*, 8577. [CrossRef] [PubMed]
26. Belon, C.; Allonas, X.; Croutxé-barghorn, C.; Lalevée, J. Overcoming the Oxygen Inhibition in the Photopolymerization of Acrylates: A Study of the Beneficial Effect of Triphenylphosphine. *J. Polym. Sci. Part A Polym. Chem.* **2010**, *48*, 2462–2469. [CrossRef]
27. Noirbent, G.; Dumur, F. Photoinitiators of Polymerization with Reduced Environmental Impact: Nature as an Unlimited and Renewable Source of Dyes. *Eur. Polym. J.* **2021**, *142*, 110109. [CrossRef]
28. Breloy, L.; Brezová, V.; Barbieriková, Z.; Ito, Y.; Akimoto, J.; Chiappone, A.; Abbad-Andaloussi, S.; Malval, J.-P.; Versace, D.-L. Methacrylated Quinizarin Derivatives for Visible-Light Mediated Photopolymerization: Promising Applications in 3D-Printing Biosourced Materials under LED@405 Nm. *ACS Appl. Polym. Mater.* **2022**, *4*, 210–228. [CrossRef]
29. Zhang, Y.; Chen, H.; Liu, S.; Josien, L.; Schrodj, G.; Simon-Masseron, A.; Lalevée, J. Photopolymerization of Pollen Based Biosourced Composites and Applications in 3D and 4D Printing. *Macromol. Mater. Eng.* **2021**, *306*, 2000774. [CrossRef]
30. Tan, N.C.S.; Djordjevic, I.; Malley, J.A.; Kwang, A.L.Q.; Ikhwan, S.; Šolić, I.; Singh, J.; Wicaksono, G.; Lim, S.; Steele, T.W.J. Sunlight Activated Film Forming Adhesive Polymers. *Mater. Sci. Eng. C* **2021**, *127*, 112240. [CrossRef]
31. Ciftci, M.; Tasdelen, M.A.; Yagci, Y. Sunlight Induced Atom Transfer Radical Polymerization by Using Dimanganese Decacarbonyl. *Polym. Chem.* **2014**, *5*, 600–606. [CrossRef]
32. Sun, K.; Chen, H.; Zhang, Y.; Morlet-Savary, F.; Graff, B.; Xiao, P.; Dumur, F.; Lalevée, J. High-Performance Sunlight Induced Polymerization Using Novel Push-Pull Dyes with High Light Absorption Properties. *Eur. Polym. J.* **2021**, *151*, 110410. [CrossRef]
33. Sun, K.; Liu, S.; Chen, H.; Morlet-Savary, F.; Graff, B.; Pigot, C.; Nechab, M.; Xiao, P.; Dumur, F.; Lalevée, J. N-Ethyl Carbazole-1-Allylidene-Based Push-Pull Dyes as Efficient Light Harvesting Photoinitiators for Sunlight Induced Polymerization. *Eur. Polym. J.* **2021**, *147*, 110331. [CrossRef]

34. Sun, K.; Pigot, C.; Zhang, Y.; Borjigin, T.; Morlet-Savary, F.; Graff, B.; Nechab, M.; Xiao, P.; Dumur, F.; Lalevée, J. Sunlight Induced Polymerization Photoinitiated by Novel Push–Pull Dyes: Indane-1,3-Dione, 1H-Cyclopenta[b]Naphthalene-1,3(2H)-Dione and 4-Dimethoxyphenyl-1-Allylidene Derivatives. *Macromol. Chem. Phys.* **2022**, *223*, 2100439. [CrossRef]
35. Dumur, F. Recent Advances on Photoinitiating Systems Designed for Solar Photocrosslinking Polymerization Reactions. *Eur. Polym. J.* **2023**, *189*, 111988. [CrossRef]
36. Dumur, F. Recent Advances on Water-Soluble Photoinitiators of Polymerization. *Eur. Polym. J.* **2023**, *189*, 111942. [CrossRef]
37. Gencoglu, T.; Eren, T.N.; Lalevée, J.; Avci, D. A Water Soluble, Low Migration, and Visible Light Photoinitiator by Thioxanthone-Functionalization of Poly(Ethylene Glycol)-Containing Poly(β-Amino Ester). *Macromol. Chem. Phys.* **2022**, *223*, 2100450. [CrossRef]
38. Aubry, B.; Dumur, F.; Lansalot, M.; Bourgeat-Lami, E.; Lacôte, E.; Lalevée, J. Development of Water-Soluble Type I Photoinitiators for Hydrogel Synthesis. *Macromol* **2022**, *2*, 131–140. [CrossRef]
39. Benedikt, S.; Wang, J.; Markovic, M.; Moszner, N.; Dietliker, K.; Ovsianikov, A.; Grützmacher, H.; Liska, R. Highly Efficient Water-Soluble Visible Light Photoinitiators. *J. Polym. Sci. Part A Polym. Chem.* **2016**, *54*, 473–479. [CrossRef]
40. Xiao, P.; Hong, W.; Li, Y.; Dumur, F.; Graff, B.; Fouassier, J.P.; Gigmes, D.; Lalevée, J. Diketopyrrolopyrrole Dyes: Structure/Reactivity/Efficiency Relationship in Photoinitiating Systems upon Visible Lights. *Polymer* **2014**, *55*, 746–751. [CrossRef]
41. Topa-Skwarczyńska, M.; Galek, M.; Jankowska, M.; Morlet-Savary, F.; Graff, B.; Lalevée, J.; Popielarz, R.; Ortyl, J. Development of the First Panchromatic BODIPY-Based One-Component Iodonium Salts for Initiating the Photopolymerization Processes. *Polym. Chem.* **2021**, *12*, 6873–6893. [CrossRef]
42. Xu, Y.; Feng, T.; Yang, T.; Wei, H.; Yang, H.; Li, G.; Zhao, M.; Liu, S.; Huang, W.; Zhao, Q. Utilizing Intramolecular Photoinduced Electron Transfer to Enhance Photothermal Tumor Treatment of Aza-BODIPY-Based Near-Infrared Nanoparticles. *ACS Appl. Mater. Interfaces* **2018**, *10*, 16299–16307. [CrossRef] [PubMed]
43. Skotnicka, A.; Kabatc, J. New BODIPY Dyes Based on Benzoxazole as Photosensitizers in Radical Polymerization of Acrylate Monomers. *Materials* **2022**, *15*, 662. [CrossRef] [PubMed]
44. Lu, P.; Chung, K.-Y.; Stafford, A.; Kiker, M.; Kafle, K.; Page, Z.A. Boron Dipyrromethene (BODIPY) in Polymer Chemistry. *Polym. Chem.* **2021**, *12*, 327–348. [CrossRef]
45. Telitel, S.; Blanchard, N.; Schweizer, S.; Morlet-Savary, F.; Graff, B.; Fouassier, J.-P.; Lalevée, J. BODIPY Derivatives and Boranil as New Photoinitiating Systems of Cationic Polymerization Exhibiting a Tunable Absorption in the 400–600 Nm Spectral Range. *Polymer* **2013**, *54*, 2071–2076. [CrossRef]
46. Telitel, S.; Lalevée, J.; Blanchard, N.; Kavalli, T.; Tehfe, M.-A.; Schweizer, S.; Morlet-Savary, F.; Graff, B.; Fouassier, J.-P. Photopolymerization of Cationic Monomers and Acrylate/Divinylether Blends under Visible Light Using Pyrromethene Dyes. *Macromolecules* **2012**, *45*, 6864–6868. [CrossRef]
47. Xiao, P.; Dumur, F.; Frigoli, M.; Graff, B.; Morlet-Savary, F.; Wantz, G.; Bock, H.; Fouassier, J.P.; Gigmes, D.; Lalevée, J. Perylene Derivatives as Photoinitiators in Blue Light Sensitive Cationic or Radical Curable Films and Panchromatic Thiol-Ene Polymerizable Films. *Eur. Polym. J.* **2014**, *53*, 215–222. [CrossRef]
48. Al Mousawi, A.; Garra, P.; Sallenave, X.; Dumur, F.; Toufaily, J.; Hamieh, T.; Graff, B.; Gigmes, D.; Fouassier, J.P.; Lalevée, J. π-Conjugated Dithienophosphole Derivatives as High Performance Photoinitiators for 3D Printing Resins. *Macromolecules* **2018**, *51*, 1811–1821. [CrossRef]
49. Barrat, A.; Simon, F.; Mazajczyk, J.; Charriere, B.; Fouquay, S.; Lalevee, J. Thiophenium Salts as New Oxidant for Redox Polymerization under Mild- and Low-Toxicity Conditions. *Molecules* **2023**, *28*, 627. [CrossRef]
50. Li, J.; Zhang, X.; Ali, S.; Akram, M.Y.; Nie, J.; Zhu, X. The Effect of Polyethylene Glycoldiacrylate Complexation on Type II Photoinitiator and Promotion for Visible Light Initiation System. *J. Photochem. Photobiol. A Chem.* **2019**, *384*, 112037. [CrossRef]
51. Li, J.; Li, S.; Li, Y.; Li, R.; Nie, J.; Zhu, X. In Situ Monitoring of Photopolymerization by Photoinitiator with Luminescence Characteristics. *J. Photochem. Photobiol. A Chem.* **2020**, *389*, 112225. [CrossRef]
52. Li, J.; Hao, Y.; Zhong, M.; Tang, L.; Nie, J.; Zhu, X. Synthesis of Furan Derivative as LED Light Photoinitiator: One-Pot, Low Usage, Photobleaching for Light Color 3D Printing. *Dye. Pigment.* **2019**, *165*, 467–473. [CrossRef]
53. Corakci, B.; Hacioglu, S.O.; Toppare, L.; Bulut, U. Long Wavelength Photosensitizers in Photoinitiated Cationic Polymerization: The Effect of Quinoxaline Derivatives on Photopolymerization. *Polymer* **2013**, *54*, 3182–3187. [CrossRef]
54. Pyszka, I.; Skowroński, Ł.; Jędrzejewska, B. Study on New Dental Materials Containing Quinoxaline-Based Photoinitiators in Terms of Exothermicity of the Photopolymerization Process. *Int. J. Mol. Sci.* **2023**, *24*, 2752. [CrossRef] [PubMed]
55. Pyszka, I.; Jędrzejewska, B. Photoinitiation Abilities of Indeno- and Indoloquinoxaline Derivatives and Mechanical Properties of Dental Fillings Based on Multifunctional Acrylic Monomers and Glass Ionomer. *Polymer* **2023**, *266*, 125625. [CrossRef]
56. Arsu, N.; Aydın, M. Photoinduced Free Radical Polymerization Initiated with Quinoxalines. *Die Angew. Makromol. Chem.* **1999**, *270*, 1–4. [CrossRef]
57. Aydın, M.; Arsu, N. Photoinitiated Free Radical Polymerization of Methylmethacrylate by Using of Quinoxalines in the Presence of Aldehydes. *Prog. Org. Coat.* **2006**, *56*, 338–342. [CrossRef]
58. Bulut, U.; Gunbas, G.E.; Toppare, L. A Quinoxaline Derivative as a Long Wavelength Photosensitizer for Diaryliodonium Salts. *J. Polym. Sci. Part A Polym. Chem.* **2010**, *48*, 209–213. [CrossRef]
59. Bulut, U.; Kolay, M.; Tarkuc, S.; Udum, Y.A.; Toppare, L. Quinoxaline Derivatives as Long Wavelength Photosensitizers in Photoinitiated Cationic Polymerization of Diaryliodonium Salts. *Prog. Org. Coat.* **2012**, *73*, 215–218. [CrossRef]

60. Cao, X.; Jin, F.; Li, Y.-F.; Chen, W.-Q.; Duan, X.-M.; Yang, L.-M. Triphenylamine-Modified Quinoxaline Derivatives as Two-Photon Photoinitiators. *New J. Chem.* **2009**, *33*, 1578–1582. [CrossRef]
61. Karaca Balta, D.; Keskin, S.; Karasu, F.; Arsu, N. Quinoxaline Derivatives as Photoinitiators in UV-Cured Coatings. *Prog. Org. Coat.* **2007**, *60*, 207–210. [CrossRef]
62. Kucybała, Z.; Pyszka, I.; Pączkowski, J. Development of New Dyeing Photoinitiators for Free Radical Polymerization Based on the 1H-Pyrazolo[3,4-b]Quinoxaline Skeleton. Part 2. *J. Chem. Soc. Perkin Trans. 2* **2000**, *7*, 1559–1567. [CrossRef]
63. Podsiadły, R.; Szymczak, A.M.; Podemska, K. The Synthesis of Novel, Visible-Wavelength, Oxidizable Polymerization Sensitizers Based on the 8-Halogeno-5,12-Dihydroquinoxalino[2,3-b]Quinoxaline Skeleton. *Dye. Pigment.* **2009**, *82*, 365–371. [CrossRef]
64. Yao, J.-Y.; Hou, H.-H.; Ma, X.-D.; Xu, H.-J.; Shi, Z.-X.; Yin, J.; Jiang, X.-S. Combining Photo-Cleavable and Hydrogen-Abstracting Groups in Quinoxaline with Thioether Bond as Hybrid Photoinitiator. *Chin. Chem. Lett.* **2017**, *28*, 6–12. [CrossRef]
65. Sun, L.; Jiang, X.; Yin, J. Study of Methoxyphenylquinoxalines (MOPQs) as Photoinitiators in the Negative Photo-Resist. *Prog. Org. Coat.* **2010**, *67*, 225–232. [CrossRef]
66. Ercan, B.T.; Gultekin, S.S.; Yesil, T.; Dincalp, H.; Koyuncu, S.; Yagci, Y.; Zafer, C. Highly Conjugated Isoindigo and Quinoxaline Dyes as Sunlight Photosensitizers for Onium Salt-Photoinitiated Cationic Polymerization of Epoxy Resins. *Polym. Int.* **2022**, *71*, 867–873. [CrossRef]
67. Dumur, F. Recent Advances on Glyoxylates and Related Structures as Photoinitiators of Polymerization. *Macromol* **2023**, *3*, 149–174. [CrossRef]
68. Launay, V.; Dumur, F.; Pieuchot, L.; Lalevée, J. Safe near Infrared Light for Fast Polymers Surface Sterilization Using Organic Heaters. *Mater. Chem. Front.* **2022**, *6*, 1172–1179. [CrossRef]
69. Bao, B.; You, J.; Li, D.; Zhan, H.; Zhang, L.; Li, M.; Wang, T. Double Benzylidene Ketones as Photoinitiators for Visible Light Photopolymerization. *J. Photochem. Photobiol. A Chem.* **2022**, *429*, 113938. [CrossRef]
70. Fu, H.; Qiu, Y.; You, J.; Hao, T.; Fan, B.; Nie, J.; Wang, T. Photopolymerization of Acrylate Resin and Ceramic Suspensions with Benzylidene Ketones under Blue/Green LED. *Polymer* **2019**, *184*, 121841. [CrossRef]
71. Zhao, Y.; Wang, W.; Wu, F.; Zhou, Y.; Huang, N.; Gu, Y.; Zou, Q.; Yang, W. Polyethylene Glycol-Functionalized Benzylidene Cyclopentanone Dyes for Two-Photon Excited Photodynamic Therapy. *Org. Biomol. Chem.* **2011**, *9*, 4168–4175. [CrossRef]
72. Fang, Y.; Liu, T.; Zou, Q.; Zhao, Y.; Wu, F. Cationic Benzylidene Cyclopentanone Photosensitizers for Selective Photodynamic Inactivation of Bacteria over Mammalian Cells. *RSC Adv.* **2015**, *5*, 56067–56074. [CrossRef]
73. Xue, J.; Zhao, Y.; Wu, F.; Fang, D.-C. Effect of Bridging Position on the Two-Photon Polymerization Initiating Efficiencies of Novel Coumarin/Benzylidene Cyclopentanone Dyes. *J. Phys. Chem. A* **2010**, *114*, 5171–5179. [CrossRef] [PubMed]
74. Abdallah, M.; Bui, T.-T.; Goubard, F.; Theodosopoulou, D.; Dumur, F.; Hijazi, A.; Fouassier, J.-P.; Lalevée, J. Phenothiazine Derivatives as Photoredox Catalysts for Cationic and Radical Photosensitive Resins for 3D Printing Technology and Photocomposite Synthesis. *Polym. Chem.* **2019**, *10*, 6145–6156. [CrossRef]
75. Zivic, N.; Bouzrati-Zerrelli, M.; Villotte, S.; Morlet-Savary, F.; Dietlin, C.; Dumur, F.; Gigmes, D.; Fouassier, J.P.; Lalevée, J. A Novel Naphthalimide Scaffold Based Iodonium Salt as a One-Component Photoacid/Photoinitiator for Cationic and Radical Polymerization under LED Exposure. *Polym. Chem.* **2016**, *7*, 5873–5879. [CrossRef]
76. Tasdelen, M.A.; Kumbaraci, V.; Jockusch, S.; Turro, N.J.; Talinli, N.; Yagci, Y. Photoacid Generation by Stepwise Two-Photon Absorption: Photoinitiated Cationic Polymerization of Cyclohexene Oxide by Using Benzodioxinone in the Presence of Iodonium Salt. *Macromolecules* **2008**, *41*, 295–297. [CrossRef]
77. Crivello, J.V.; Lam, J.H.W. Diaryliodonium Salts. A New Class of Photoinitiators for Cationic Polymerization. *Macromolecules* **1977**, *10*, 1307–1315. [CrossRef]
78. He, Y.; Zhou, W.; Wu, F.; Li, M.; Wang, E. Photoreaction and Photopolymerization Studies on Squaraine Dyes/Iodonium Salts Combination. *J. Photochem. Photobiol. A Chem.* **2004**, *162*, 463–471. [CrossRef]
79. Jun, L.I.; Miaozhen, L.I.; Huaihai, S.; Yongyuan, Y.; Erjian, W. Photopolymerization Initiated by Dimethylaminochalcone/Diphenyliodonium Salt Combination System Sensitive to Visible Light. *Chin. J. Polym. Sci.* **1993**, *11*, 163–170.
80. Petko, F.; Galek, M.; Hola, E.; Topa-Skwarczyńska, M.; Tomal, W.; Jankowska, M.; Pilch, M.; Popielarz, R.; Graff, B.; Morlet-Savary, F.; et al. Symmetric Iodonium Salts Based on Benzylidene as One-Component Photoinitiators for Applications in 3D Printing. *Chem. Mater.* **2022**, *34*, 10077–10092. [CrossRef]
81. Petko, F.; Galek, M.; Hola, E.; Popielarz, R.; Ortyl, J. One-Component Cationic Photoinitiators from Tunable Benzylidene Scaffolds for 3D Printing Applications. *Macromolecules* **2021**, *54*, 7070–7087. [CrossRef]
82. Zhang, J.; Dumur, F.; Xiao, P.; Graff, B.; Bardelang, D.; Gigmes, D.; Fouassier, J.P.; Lalevée, J. Structure Design of Naphthalimide Derivatives: Toward Versatile Photoinitiators for Near-UV/Visible LEDs, 3D Printing, and Water-Soluble Photoinitiating Systems. *Macromolecules* **2015**, *48*, 2054–2063. [CrossRef]
83. Xiao, P.; Dumur, F.; Frigoli, M.; Tehfe, M.-A.; Graff, B.; Fouassier, J.P.; Gigmes, D.; Lalevée, J. Naphthalimide Based Methacrylated Photoinitiators in Radical and Cationic Photopolymerization under Visible Light. *Polym. Chem.* **2013**, *4*, 5440–5448. [CrossRef]
84. Zivic, N.; Zhang, J.; Bardelang, D.; Dumur, F.; Xiao, P.; Jet, T.; Versace, D.-L.; Dietlin, C.; Morlet-Savary, F.; Graff, B.; et al. Novel Naphthalimide–Amine Based Photoinitiators Operating under Violet and Blue LEDs and Usable for Various Polymerization Reactions and Synthesis of Hydrogels. *Polym. Chem.* **2015**, *7*, 418–429. [CrossRef]
85. Xiao, P.; Dumur, F.; Graff, B.; Morlet-Savary, F.; Gigmes, D.; Fouassier, J.P.; Lalevée, J. Design of High Performance Photoinitiators at 385–405 Nm: Search around the Naphthalene Scaffold. *Macromolecules* **2014**, *47*, 973–978. [CrossRef]

86. Dumur, F. Recent Advances on Visible Light Triphenylamine-Based Photoinitiators of Polymerization. *Eur. Polym. J.* **2022**, *166*, 111036. [CrossRef]
87. Hsieh, J.-B.; Yen, S.-C.; Hammoud, F.; Lalevée, J.; Chen, Y.-C. Effect of Terminal Alkyl Chains for Free Radical Photopolymerization Based on Triphenylamine Oxime Ester Visible-Light Absorbing Type I Photoinitiators. *ChemistrySelect* **2023**, *8*, e202301297. [CrossRef]
88. Wu, Y.-H.; Noon, A.; Hammoud, F.; Hamieh, T.; Toufaily, J.; Graff, B.; Lalevée, J.; Chen, Y.-C. Multibranched Triarylamine End-Capped Oxime Esters as Visible-Light Absorbing Type I Photoinitiators for Free Radical Photopolymerization. *Polym. Chem.* **2023**, *14*, 3421–3432. [CrossRef]
89. Noirbent, G.; Xu, Y.; Bonardi, A.-H.; Duval, S.; Gigmes, D.; Lalevée, J.; Dumur, F. New Donor-Acceptor Stenhouse Adducts as Visible and Near Infrared Light Polymerization Photoinitiators. *Molecules* **2020**, *25*, 2317. [CrossRef]
90. Ma, Q.; Buchon, L.; Magné, V.; Graff, B.; Morlet-Savary, F.; Xu, Y.; Benltifa, M.; Lakhdar, S.; Lalevée, J. Charge Transfer Complexes (CTCs) with Pyridinium Salts: Toward Efficient Dual Photochemical/Thermal Initiators and 3D Printing Applications. *Macromol. Rapid Commun.* **2022**, *43*, 2200314. [CrossRef]
91. Mousawi, A.A.; Dumur, F.; Garra, P.; Toufaily, J.; Hamieh, T.; Goubard, F.; Bui, T.-T.; Graff, B.; Gigmes, D.; Fouassier, J.P.; et al. Azahelicenes as Visible Light Photoinitiators for Cationic and Radical Polymerization: Preparation of Photoluminescent Polymers and Use in High Performance LED Projector 3D Printing Resins. *J. Polym. Sci. Part A Polym. Chem.* **2017**, *55*, 1189–1199. [CrossRef]
92. El-Roz, M.; Lalevée, J.; Allonas, X.; Fouassier, J.P. Mechanistic Investigation of the Silane, Germane, and Stannane Behavior When Incorporated in Type I and Type II Photoinitiators of Polymerization in Aerated Media. *Macromolecules* **2009**, *42*, 8725–8732. [CrossRef]
93. Lalevée, J.; Dirani, A.; El-Roz, M.; Allonas, X.; Fouassier, J.P. Germanes as Efficient Coinitiators in Radical and Cationic Photopolymerizations. *J. Polym. Sci. Part A Polym. Chem.* **2008**, *46*, 3042–3047. [CrossRef]
94. Helmy, S.; Oh, S.; Leibfarth, F.A.; Hawker, C.J.; Read de Alaniz, J. Design and Synthesis of Donor–Acceptor Stenhouse Adducts: A Visible Light Photoswitch Derived from Furfural. *J. Org. Chem.* **2014**, *79*, 11316–11329. [CrossRef] [PubMed]
95. Pigot, C.; Noirbent, G.; Brunel, D.; Dumur, F. Recent Advances on Push–Pull Organic Dyes as Visible Light Photoinitiators of Polymerization. *Eur. Polym. J.* **2020**, *133*, 109797. [CrossRef]
96. Tehfe, M.-A.; Dumur, F.; Contal, E.; Graff, B.; Gigmes, D.; Fouassier, J.-P.; Lalevée, J. Novel Highly Efficient Organophotocatalysts: Truxene–Acridine-1,8-Diones as Photoinitiators of Polymerization. *Macromol. Chem. Phys.* **2013**, *214*, 2189–2201. [CrossRef]
97. Tehfe, M.-A.; Dumur, F.; Telitel, S.; Gigmes, D.; Contal, E.; Bertin, D.; Morlet-Savary, F.; Graff, B.; Fouassier, J.-P.; Lalevée, J. Zinc-Based Metal Complexes as New Photocatalysts in Polymerization Initiating Systems. *Eur. Polym. J.* **2013**, *49*, 1040–1049. [CrossRef]
98. Chen, H.; Zhu, D.; Kavalli, T.; Xiao, P.; Schmitt, M.; Lalevée, J. Photopolymerization Using Bio-Sourced Photoinitiators. *Polym. Chem.* **2023**, *14*, 3543–3568. [CrossRef]
99. Xiao, P.; Dumur, F.; Zhang, J.; Gigmes, D.; Fouassier, J.P.; Lalevée, J. Copper Complexes: The Effect of Ligands on Their Photoinitiation Efficiencies in Radical Polymerization Reactions under Visible Light. *Polym. Chem.* **2014**, *5*, 6350–6357. [CrossRef]
100. Xiao, P.; Zhang, J.; Campolo, D.; Dumur, F.; Gigmes, D.; Fouassier, J.P.; Lalevée, J. Copper and Iron Complexes as Visible-Light-Sensitive Photoinitiators of Polymerization. *J. Polym. Sci. Part A Polym. Chem.* **2015**, *53*, 2673–2684. [CrossRef]
101. Bouzrati-Zerelli, M.; Guillaume, N.; Goubard, F.; Bui, T.-T.; Villotte, S.; Dietlin, C.; Morlet-Savary, F.; Gigmes, D.; Fouassier, J.P.; Dumur, F.; et al. A Novel Class of Photoinitiators with a Thermally Activated Delayed Fluorescence (TADF) Property. *New J. Chem.* **2018**, *42*, 8261–8270. [CrossRef]
102. Li, B.; Lalevée, J.; Mazur, L.M.; Matczyszyn, K.; Ravaine, S.; Jradi, S. Copper Complex-Based Photoinitiator for High Resolution Two-Photon Polymerization. *Addit. Manuf.* **2023**, *75*, 103741. [CrossRef]
103. Alhomaidan, L.M.; Tar, H.; Alnafisah, A.S.; Aroua, L.M.; KouKi, N.; Alminderej, F.M.; Lalevee, J. Copper II Complexes Based on Benzimidazole Ligands as a Novel Photoredox Catalysis for Free Radical Polymerization Embedded Gold and Silver Nanoparticles. *Polymers* **2023**, *15*, 1289. [CrossRef] [PubMed]
104. Fouassier, J.P.; Morlet-Savary, F.; Yamashita, K.; Imahashi, S. The Role of the Dye/Iron Arene Complex/Amine System as a Photoinitiator for Photopolymerization Reactions. *Polymer* **1997**, *38*, 1415–1421. [CrossRef]
105. Telitel, S.; Dumur, F.; Campolo, D.; Poly, J.; Gigmes, D.; Fouassier, J.P.; Lalevée, J. Iron Complexes as Potential Photocatalysts for Controlled Radical Photopolymerizations: A Tool for Modifications and Patterning of Surfaces. *J. Polym. Sci. Part A Polym. Chem.* **2016**, *54*, 702–713. [CrossRef]
106. Karaca, N.; Ocal, N.; Arsu, N.; Jockusch, S. Thioxanthone-Benzothiophenes as Photoinitiator for Free Radical Polymerization. *J. Photochem. Photobiol. A Chem.* **2016**, *331*, 22–28. [CrossRef]
107. Balta, D.K.; Cetiner, N.; Temel, G.; Turgut, Z.; Arsu, N. An Annelated Thioxanthone as a New Type II Initiator. *J. Photochem. Photobiol. A Chem.* **2008**, *199*, 316–321. [CrossRef]
108. Balta, D.K.; Temel, G.; Goksu, G.; Ocal, N.; Arsu, N. Thioxanthone–Diphenyl Anthracene: Visible Light Photoinitiator. *Macromolecules* **2012**, *45*, 119–125. [CrossRef]
109. Dadashi-Silab, S.; Aydogan, C.; Yagci, Y. Shining a Light on an Adaptable Photoinitiator: Advances in Photopolymerizations Initiated by Thioxanthones. *Polym. Chem.* **2015**, *6*, 6595–6615. [CrossRef]

110. Eren, T.N.; Yasar, N.; Aviyente, V.; Morlet-Savary, F.; Graff, B.; Fouassier, J.P.; Lalevee, J.; Avci, D. Photophysical and Photochemical Studies of Novel Thioxanthone-Functionalized Methacrylates through LED Excitation. *Macromol. Chem. Phys.* **2016**, *217*, 1501–1512. [CrossRef]
111. Qiu, J.; Wei, J. Thioxanthone Photoinitiator Containing Polymerizable N-Aromatic Maleimide for Photopolymerization. *J. Polym. Res.* **2014**, *21*, 559. [CrossRef]
112. Tar, H.; Sevinc Esen, D.; Aydin, M.; Ley, C.; Arsu, N.; Allonas, X. Panchromatic Type II Photoinitiator for Free Radical Polymerization Based on Thioxanthone Derivative. *Macromolecules* **2013**, *46*, 3266–3272. [CrossRef]
113. Wu, Q.; Wang, X.; Xiong, Y.; Yang, J.; Tang, H. Thioxanthone Based One-Component Polymerizable Visible Light Photoinitiator for Free Radical Polymerization. *RSC Adv.* **2016**, *6*, 66098–66107. [CrossRef]
114. Wu, Q.; Tang, K.; Xiong, Y.; Wang, X.; Yang, J.; Tang, H. High-Performance and Low Migration One-Component Thioxanthone Visible Light Photoinitiators. *Macromol. Chem. Phys.* **2017**, *218*, 1600484. [CrossRef]
115. Wu, X.; Jin, M.; Malval, J.-P.; Wan, D.; Pu, H. Visible Light-Emitting Diode-Sensitive Thioxanthone Derivatives Used in Versatile Photoinitiating Systems for Photopolymerizations. *J. Polym. Sci. Part A Polym. Chem.* **2017**, *55*, 4037–4045. [CrossRef]
116. Esen, D.S.; Karasu, F.; Arsu, N. The Investigation of Photoinitiated Polymerization of Multifunctional Acrylates with TX-BT by Photo-DSC and RT-FTIR. *Prog. Org. Coat.* **2011**, *70*, 102–107. [CrossRef]
117. Lalevée, J.; Blanchard, N.; Tehfe, M.A.; Fries, C.; Morlet-Savary, F.; Gigmes, D.; Fouassier, J.P. New Thioxanthone and Xanthone Photoinitiators Based on Silyl Radical Chemistry. *Polym. Chem.* **2011**, *2*, 1077–1084. [CrossRef]
118. Wang, Y.; Chen, R.; Liu, D.; Peng, C.; Wang, J.; Dong, X. New Functionalized Thioxanthone Derivatives as Type I Photoinitiators for Polymerization under UV-Vis LEDs. *New J. Chem.* **2023**, *47*, 5330–5337. [CrossRef]
119. Dumur, F. Recent Advances on Furan-Based Visible Light Photoinitiators of Polymerization. *Catalysts* **2023**, *13*, 493. [CrossRef]
120. Kamoun, E.A.; Winkel, A.; Eisenburger, M.; Menzel, H. Carboxylated Camphorquinone as Visible-Light Photoinitiator for Biomedical Application: Synthesis, Characterization, and Application. *Arab. J. Chem.* **2016**, *9*, 745–754. [CrossRef]
121. Santini, A.; Gallegos, I.T.; Felix, C.M. Photoinitiators in Dentistry: A Review. *Prim. Dent. J.* **2013**, *2*, 30–33. [CrossRef]
122. Dumur, F. Recent Advances on Anthracene-Based Photoinitiators of Polymerization. *Eur. Polym. J.* **2022**, *169*, 111139. [CrossRef]
123. Liu, S.; Brunel, D.; Sun, K.; Xu, Y.; Morlet-Savary, F.; Graff, B.; Xiao, P.; Dumur, F.; Lalevée, J. A Monocomponent Bifunctional Benzophenone–Carbazole Type II Photoinitiator for LED Photoinitiating Systems. *Polym. Chem.* **2020**, *11*, 3551–3556. [CrossRef]
124. Lalevée, J.; Allonas, X.; Fouassier, J.-P. Reactivity of Carbon-Centered Radicals toward Acrylate Double Bonds: Relative Contribution of Polar vs Enthalpy Effects. *J. Phys. Chem. A* **2004**, *108*, 4326–4334. [CrossRef]
125. Chen, H.; Noirbent, G.; Sun, K.; Brunel, D.; Gigmes, D.; Morlet-Savary, F.; Zhang, Y.; Liu, S.; Xiao, P.; Dumur, F.; et al. Photoinitiators Derived from Natural Product Scaffolds: Monochalcones in Three-Component Photoinitiating Systems and Their Applications in 3D Printing. *Polym. Chem.* **2020**, *11*, 4647–4659. [CrossRef]
126. Tang, L.; Nie, J.; Zhu, X. A High Performance Phenyl-Free LED Photoinitiator for Cationic or Hybrid Photopolymerization and Its Application in LED Cationic 3D Printing. *Polym. Chem.* **2020**, *11*, 2855–2863. [CrossRef]
127. Chen, H.; Noirbent, G.; Liu, S.; Brunel, D.; Graff, B.; Gigmes, D.; Zhang, Y.; Sun, K.; Morlet-Savary, F.; Xiao, P.; et al. Bis-Chalcone Derivatives Derived from Natural Products as near-UV/Visible Light Sensitive Photoinitiators for 3D/4D Printing. *Mater. Chem. Front.* **2021**, *5*, 901–916. [CrossRef]
128. Sun, K.; Xu, Y.; Dumur, F.; Morlet-Savary, F.; Chen, H.; Dietlin, C.; Graff, B.; Lalevée, J.; Xiao, P. In Silico Rational Design by Molecular Modeling of New Ketones as Photoinitiators in Three-Component Photoinitiating Systems: Application in 3D Printing. *Polym. Chem.* **2020**, *11*, 2230–2242. [CrossRef]
129. Yen, S.-C.; Ni, J.-S.; Chen, Y.-C. Triphenylamine-Functionalized Chalcones as One-Component Type II Visible-Light-Absorbing Photoinitiators for Free Radical Photopolymerization. *Eur. Polym. J.* **2023**, *187*, 111885. [CrossRef]
130. Gao, Y.; Qu, J. New Long-Wavelength D–π-A–π-D Chalcone Photoinitiator for Visible Light Polymerization with Photobleaching and Biocompatibility Properties. *Polym. Chem.* **2023**, *14*, 952–962. [CrossRef]
131. Deng, L.; Qu, J. Synthesis and Properties of Novel Bis-Chalcone-Based Photoinitiators for LED Polymerization with Photobleaching and Low Migration. *Prog. Org. Coat.* **2023**, *174*, 107240. [CrossRef]
132. Hola, E.; Morlet-Savary, F.; Lalevée, J.; Ortyl, J. Photoinitiator or Photosensitizer? Dual Behaviour of m-Terphenyls in Photopolymerization Processes. *Eur. Polym. J.* **2023**, *189*, 111971. [CrossRef]
133. Ma, Q.; Zhang, X.; Liu, Y.; Graff, B.; Lalevee, J. Dual Photo/Thermal Initiation with Charge Transfer Complexes Based on Bromide-Based Electron Acceptors. *J. Polym. Sci.* **2023**, *61*, 741–747. [CrossRef]
134. Bonardi, A.; Bonardi, F.; Noirbent, G.; Dumur, F.; Dietlin, C.; Gigmes, D.; Fouassier, J.-P.; Lalevée, J. Different NIR Dye Scaffolds for Polymerization Reactions under NIR Light. *Polym. Chem.* **2019**, *10*, 6505–6514. [CrossRef]
135. Uchida, N.; Nakano, H.; Igarashi, T.; Sakurai, T. Nonsalt 1-(Arylmethyloxy)Pyrene Photoinitiators Capable of Initiating Cationic Polymerization. *J. Appl. Polym. Sci.* **2014**, *131*, 40510. [CrossRef]
136. Mishra, A.; Daswal, S. 1-(Bromoacetyl)Pyrene, a Novel Photoinitiator for the Copolymerization of Styrene and Methylmethacrylate. *Radiat. Phys. Chem.* **2006**, *75*, 1093–1100. [CrossRef]
137. Dumur, F. Recent Advances on Pyrene-Based Photoinitiators of Polymerization. *Eur. Polym. J.* **2020**, *126*, 109564. [CrossRef]
138. Zhang, J.; Campolo, D.; Dumur, F.; Xiao, P.; Gigmes, D.; Fouassier, J.P.; Lalevée, J. The Carbazole-Bound Ferrocenium Salt as a Specific Cationic Photoinitiator upon near-UV and Visible LEDs (365–405 Nm). *Polym. Bull.* **2016**, *73*, 493–507. [CrossRef]

139. Al Mousawi, A.; Garra, P.; Dumur, F.; Bui, T.-T.; Goubard, F.; Toufaily, J.; Hamieh, T.; Graff, B.; Gigmes, D.; Fouassier, J.P.; et al. Novel Carbazole Skeleton-Based Photoinitiators for LED Polymerization and LED Projector 3D Printing. *Molecules* **2017**, *22*, 2143. [CrossRef]
140. Abdallah, M.; Magaldi, D.; Hijazi, A.; Graff, B.; Dumur, F.; Fouassier, J.-P.; Bui, T.-T.; Goubard, F.; Lalevée, J. Development of New High-Performance Visible Light Photoinitiators Based on Carbazole Scaffold and Their Applications in 3d Printing and Photocomposite Synthesis. *J. Polym. Sci. Part A Polym. Chem.* **2019**, *57*, 2081–2092. [CrossRef]
141. Liao, W.; Liao, Q.; Xiong, Y.; Li, Z.; Tang, H. Design, Synthesis and Properties of Carbazole-Indenedione Based Photobleachable Photoinitiators for Photopolymerization. *J. Photochem. Photobiol. A Chem.* **2023**, *435*, 114297. [CrossRef]
142. Bin, F.-C.; Guo, M.; Li, T.; Zheng, Y.-C.; Dong, X.-Z.; Liu, J.; Jin, F.; Zheng, M.-L. Carbazole-Based Anion Ionic Water-Soluble Two-Photon Initiator for Achieving 3D Hydrogel Structures. *Adv. Funct. Mater.* **2023**, *33*, 2300293. [CrossRef]
143. Chen, Q.; Yang, Q.; Gao, P.; Chi, B.; Nie, J.; He, Y. Photopolymerization of Coumarin-Containing Reversible Photoresponsive Materials Based on Wavelength Selectivity. *Ind. Eng. Chem. Res.* **2019**, *58*, 2970–2975. [CrossRef]
144. Li, Z.; Zou, X.; Zhu, G.; Liu, X.; Liu, R. Coumarin-Based Oxime Esters: Photobleachable and Versatile Unimolecular Initiators for Acrylate and Thiol-Based Click Photopolymerization under Visible Light-Emitting Diode Light Irradiation. *ACS Appl. Mater. Interfaces* **2018**, *10*, 16113–16123. [CrossRef]
145. Rajeshirke, M.; Sreenath, M.C.; Chitrambalam, S.; Joe, I.H.; Sekar, N. Enhancement of NLO Properties in OBO Fluorophores Derived from Carbazole–Coumarin Chalcones Containing Carboxylic Acid at the N-Alykl Terminal End. *J. Phys. Chem. C* **2018**, *122*, 14313–14325. [CrossRef]
146. Zhu, Y.; Li, L.; Zhang, Y.; Ou, Y.; Zhang, J.; Yagci, Y.; Liu, R. Broad Wavelength Sensitive Coumarin Sulfonium Salts as Photoinitiators for Cationic, Free Radical and Hybrid Photopolymerizations. *Prog. Org. Coat.* **2023**, *174*, 107272. [CrossRef]
147. Nzulu, F.; Telitel, S.; Stoffelbach, F.; Graff, B.; Morlet-Savary, F.; Lalevée, J.; Fensterbank, L.; Goddard, J.-P.; Ollivier, C. A Dinuclear Gold(i) Complex as a Novel Photoredox Catalyst for Light-Induced Atom Transfer Radical Polymerization. *Polym. Chem.* **2015**, *6*, 4605–4611. [CrossRef]
148. Tehfe, M.-A.; Lepeltier, M.; Dumur, F.; Gigmes, D.; Fouassier, J.-P.; Lalevée, J. Structural Effects in the Iridium Complex Series: Photoredox Catalysis and Photoinitiation of Polymerization Reactions under Visible Lights. *Macromol. Chem. Phys.* **2017**, *218*, 1700192. [CrossRef]
149. Zhao, J.; Lalevée, J.; Lu, H.; MacQueen, R.; Kable, S.H.; Schmidt, T.W.; Stenzel, M.H.; Xiao, P. A New Role of Curcumin: As a Multicolor Photoinitiator for Polymer Fabrication under Household UV to Red LED Bulbs. *Polym. Chem.* **2015**, *6*, 5053–5061. [CrossRef]
150. Crivello, J.V.; Bulut, U. Curcumin: A Naturally Occurring Long-Wavelength Photosensitizer for Diaryliodonium Salts. *J. Polym. Sci. Part A Polym. Chem.* **2005**, *43*, 5217–5231. [CrossRef]
151. Han, W.; Fu, H.; Xue, T.; Liu, T.; Wang, Y.; Wang, T. Facilely Prepared Blue-Green Light Sensitive Curcuminoids with Excellent Bleaching Properties as High Performance Photosensitizers in Cationic and Free Radical Photopolymerization. *Polym. Chem.* **2018**, *9*, 1787–1798. [CrossRef]
152. Mishra, A.; Daswal, S. Curcumin, A Novel Natural Photoinitiator for the Copolymerization of Styrene and Methylmethacrylate. *J. Macromol. Sci. Part A* **2005**, *42*, 1667–1678. [CrossRef]
153. Dumur, F. Recent Advances on Anthraquinone-Based Photoinitiators of Polymerization. *Eur. Polym. J.* **2023**, *191*, 112039. [CrossRef]
154. Zhang, J.; Lalevée, J.; Zhao, J.; Graff, B.; Stenzel, M.H.; Xiao, P. Dihydroxyanthraquinone Derivatives: Natural Dyes as Blue-Light-Sensitive Versatile Photoinitiators of Photopolymerization. *Polym. Chem.* **2016**, *7*, 7316–7324. [CrossRef]
155. Xiao, P.; Dumur, F.; Graff, B.; Fouassier, J.P.; Gigmes, D.; Lalevée, J. Cationic and Thiol–Ene Photopolymerization upon Red Lights Using Anthraquinone Derivatives as Photoinitiators. *Macromolecules* **2013**, *46*, 6744–6750. [CrossRef]
156. Dumur, F. Recent Advances on Naphthoquinone-Based Photoinitiators of Polymerization. *Eur. Polym. J.* **2023**, *193*, 112120. [CrossRef]
157. Addi, M.; Elbouzidi, A.; Abid, M.; Tungmunnithum, D.; Elamrani, A.; Hano, C. An Overview of Bioactive Flavonoids from Citrus Fruits. *Appl. Sci.* **2022**, *12*, 29. [CrossRef]
158. Panche, A.N.; Diwan, A.D.; Chandra, S.R. Flavonoids: An Overview. *J. Nutr. Sci.* **2016**, *5*, e47. [CrossRef] [PubMed]
159. Tomás-Barberán, F.A.; Tomás-Lorente, F.; Ferreres, F.; Garcia-Viguera, C. Flavonoids as Biochemical Markers of the Plant Origin of Bee Pollen. *J. Sci. Food Agric.* **1989**, *47*, 337–340. [CrossRef]
160. Levy, M.; Levin, D.A. The Origin of Novel Flavonoids in Phlox Allotetraploids. *Proc. Natl. Acad. Sci. USA* **1971**, *68*, 1627–1630. [CrossRef]
161. Tomás-Barberán, F.A.; Ferreres, F.; García-Vignera, C.; Tomás-Lorente, F. Flavonoids in Honey of Different Geographical Origin. *Z. Für Lebensm.-Unters. Und Forsch.* **1993**, *196*, 38–44. [CrossRef]
162. Chebil, L.; Anthoni, J.; Humeau, C.; Gerardin, C.; Engasser, J.-M.; Ghoul, M. Enzymatic Acylation of Flavonoids: Effect of the Nature of the Substrate, Origin of Lipase, and Operating Conditions on Conversion Yield and Regioselectivity. *J. Agric. Food Chem.* **2007**, *55*, 9496–9502. [CrossRef] [PubMed]
163. Nunes, A.R.; Vieira, Í.G.P.; Queiroz, D.B.; Leal, A.L.A.B.; Maia Morais, S.; Muniz, D.F.; Calixto-Junior, J.T.; Coutinho, H.D.M. Use of Flavonoids and Cinnamates, the Main Photoprotectors with Natural Origin. *Adv. Pharmacol. Sci.* **2018**, *2018*, 5341487. [CrossRef] [PubMed]

164. Lima, B.; Tapia, A.; Luna, L.; Fabani, M.P.; Schmeda-Hirschmann, G.; Podio, N.S.; Wunderlin, D.A.; Feresin, G.E. Main Flavonoids, DPPH Activity, and Metal Content Allow Determination of the Geographical Origin of Propolis from the Province of San Juan (Argentina). *J. Agric. Food Chem.* **2009**, *57*, 2691–2698. [CrossRef] [PubMed]
165. Santos, E.L.; Maia, B.H.L.N.S.; Ferriani, A.P.; Teixeira, S.D. Flavonoids: Classification, Biosynthesis and Chemical Ecology. In *Flavonoids*; Justino, G.C., Ed.; IntechOpen: Rijeka, Croatia, 2017; p. Ch. 1, ISBN 978-953-51-3424-4.
166. Harborne, J.B.; Williams, C.A. Advances in Flavonoid Research since 1992. *Phytochemistry* **2000**, *55*, 481–504. [CrossRef] [PubMed]
167. Pecorini, G.; Ferraro, E.; Puppi, D. Polymeric Systems for the Controlled Release of Flavonoids. *Pharmaceutics* **2023**, *15*, 628. [CrossRef] [PubMed]
168. Al-Khayri, J.M.; Sahana, G.R.; Nagella, P.; Joseph, B.V.; Alessa, F.M.; Al-Mssallem, M.Q. Flavonoids as Potential Anti-Inflammatory Molecules: A Review. *Molecules* **2022**, *27*, 2901. [CrossRef] [PubMed]
169. Ortiz, A.D.; Fideles, S.O.; Reis, C.H.; Bellini, M.Z.; Pereira, E.D.; Pilon, J.P.; de Marchi, M.Â.; Detregiachi, C.R.; Flato, U.A.; Trazzi, B.F.; et al. Therapeutic Effects of Citrus Flavonoids Neohesperidin, Hesperidin and Its Aglycone, Hesperetin on Bone Health. *Biomolecules* **2022**, *12*, 626. [CrossRef] [PubMed]
170. Wen, K.; Fang, X.; Yang, J.; Yao, Y.; Nandakumar, S.K.; Salem, L.M.; Cheng, K. Recent Research on Flavonoids and Their Biomedical Applications. *Curr. Med. Chem.* **2021**, *28*, 1042–1066. [CrossRef]
171. Ullah, A.; Munir, S.; Badshah, S.L.; Khan, N.; Ghani, L.; Poulson, B.G.; Emwas, A.-H.; Jaremko, M. Important Flavonoids and Their Role as a Therapeutic Agent. *Molecules* **2020**, *25*, 5243. [CrossRef]
172. Tzanova, M.; Atanasov, V.; Yaneva, Z.; Ivanova, D.; Dinev, T. Selectivity of Current Extraction Techniques for Flavonoids from Plant Materials. *Processes* **2020**, *8*, 1222. [CrossRef]
173. Giacoletto, N.; Dumur, F. Recent Advances in Bis-Chalcone-Based Photoinitiators of Polymerization: From Mechanistic Investigations to Applications. *Molecules* **2021**, *26*, 3192. [CrossRef]
174. Ibrahim-Ouali, M.; Dumur, F. Recent Advances on Chalcone-Based Photoinitiators of Polymerization. *Eur. Polym. J.* **2021**, *158*, 110688. [CrossRef]
175. Lago, M.A.; Quirós, A.R.-B.d.; Sendón, R.; Bustos, J.; Nieto, M.T.; Paseiro, P. Photoinitiators: A Food Safety Review. *Food Addit. Contam. Part A* **2015**, *32*, 779–798. [CrossRef] [PubMed]
176. Hammoud, F.; Hijazi, A.; Schmitt, M.; Dumur, F.; Lalevée, J. A Review on Recently Proposed Oxime Ester Photoinitiators. *Eur. Polym. J.* **2023**, *188*, 111901. [CrossRef]
177. Sun, K.; Xiao, P.; Dumur, F.; Lalevée, J. Organic Dye-Based Photoinitiating Systems for Visible-Light-Induced Photopolymerization. *J. Polym. Sci.* **2021**, *59*, 1338–1389. [CrossRef]
178. Tehfe, M.-A.; Dumur, F.; Xiao, P.; Graff, B.; Morlet-Savary, F.; Fouassier, J.-P.; Gigmes, D.; Lalevée, J. New Chromone Based Photoinitiators for Polymerization Reactions under Visible Light. *Polym. Chem.* **2013**, *4*, 4234–4244. [CrossRef]
179. Rao, Y.J.; Sowjanya, T.; Thirupathi, G.; Murthy, N.Y.S.; Kotapalli, S.S. Synthesis and Biological Evaluation of Novel Flavone/Triazole/Benzimidazole Hybrids and Flavone/Isoxazole-Annulated Heterocycles as Antiproliferative and Antimycobacterial Agents. *Mol. Divers.* **2018**, *22*, 803–814. [CrossRef]
180. Yu, H.; Kim, S.-H.; Lee, J.-Y.; Kim, H.-J.; Seo, S.-H.; Chung, B.-Y.; Jin, C.-B.; Lee, Y.-S. Synthesis and Antioxidant Activity of 3-Methoxyflavones. *Bull. Korean Chem. Soc.* **2005**, *26*, 2057–2060.
181. Balasuriya, N.; Rupasinghe, H.P.V. Antihypertensive Properties of Flavonoid-Rich Apple Peel Extract. *Food Chem.* **2012**, *135*, 2320–2325. [CrossRef]
182. Li, J.-X.; Xue, B.; Chai, Q.; Liu, Z.-X.; Zhao, A.-P.; Chen, L.-B. Antihypertensive Effect of Total Flavonoid Fraction of Astragalus Complanatus in Hypertensive Rats. *Chin. J. Physiol.* **2005**, *48*, 101–106.
183. Kawai, M.; Hirano, T.; Higa, S.; Arimitsu, J.; Maruta, M.; Kuwahara, Y.; Ohkawara, T.; Hagihara, K.; Yamadori, T.; Shima, Y.; et al. Flavonoids and Related Compounds as Anti-Allergic Substances. *Allergol. Int.* **2007**, *56*, 113–123. [CrossRef] [PubMed]
184. Orhan, D.D.; Özçelik, B.; Özgen, S.; Ergun, F. Antibacterial, Antifungal, and Antiviral Activities of Some Flavonoids. *Microbiol. Res.* **2010**, *165*, 496–504. [CrossRef] [PubMed]
185. Inoue, T.; Sugimoto, Y.; Masuda, H.; Kamei, C. Antiallergic Effect of Flavonoid Glycosides Obtained from *Mentha piperita* L. *Biol. Pharm. Bull.* **2002**, *25*, 256–259. [CrossRef] [PubMed]
186. Nijveldt, R.J.; van Nood, E.; van Hoorn, D.E.; Boelens, P.G.; van Norren, K.; van Leeuwen, P.A. Flavonoids: A Review of Probable Mechanisms of Action and Potential Applications123. *Am. J. Clin. Nutr.* **2001**, *74*, 418–425. [CrossRef] [PubMed]
187. Forbes, A.M.; Lin, H.; Meadows, G.G.; Meier, G.P. Synthesis and Anticancer Activity of New Flavonoid Analogs and Inconsistencies in Assays Related to Proliferation and Viability Measurements. *Int. J. Oncol.* **2014**, *45*, 831–842. [CrossRef] [PubMed]
188. Merzlyak, M.N.; Solovchenko, A.E.; Smagin, A.I.; Gitelson, A.A. Apple Flavonols during Fruit Adaptation to Solar Radiation: Spectral Features and Technique for Non-Destructive Assessment. *J. Plant Physiol.* **2005**, *162*, 151–160. [CrossRef] [PubMed]
189. Tamer, Ö.; Şimşek, M.; Avcı, D.; Atalay, Y. First and Second Order Hyperpolarizabilities of Flavonol Derivatives: A Density Functional Theory Study. *Spectrochim. Acta Part A Mol. Biomol. Spectrosc.* **2022**, *283*, 121728. [CrossRef]
190. Yuan, H.; Jiang, A.; Fang, H.; Chen, Y.; Guo, Z. Optical Properties of Natural Small Molecules and Their Applications in Imaging and Nanomedicine. *Adv. Drug Deliv. Rev.* **2021**, *179*, 113917. [CrossRef]
191. Yang, Q.; Muchová, L.; Štacková, L.; Štacko, P.; Šindelář, V.; Vítek, L.; Klán, P. Cyanine–Flavonol Hybrids as NIR-Light Activatable Carbon Monoxide Donors in Methanol and Aqueous Solutions. *Chem. Commun.* **2022**, *58*, 8958–8961. [CrossRef]

192. Höfener, S.; Kooijman, P.C.; Groen, J.; Ariese, F.; Visscher, L. Fluorescence Behavior of (Selected) Flavonols: A Combined Experimental and Computational Study. *Phys. Chem. Chem. Phys.* **2013**, *15*, 12572–12581. [CrossRef]
193. Sengupta, P.K.; Kasha, M. Excited State Proton-Transfer Spectroscopy of 3-Hydroxyflavone and Quercetin. *Chem. Phys. Lett.* **1979**, *68*, 382–385. [CrossRef]
194. Strandjord, A.J.G.; Courtney, S.H.; Friedrich, D.M.; Barbara, P.F. Excited-State Dynamics of 3-Hydroxyflavone. *J. Phys. Chem.* **1983**, *87*, 1125–1133. [CrossRef]
195. McMorrow, D.; Kasha, M. Intramolecular Excited-State Proton Transfer in 3-Hydroxyflavone. Hydrogen-Bonding Solvent Perturbations. *J. Phys. Chem.* **1984**, *88*, 2235–2243. [CrossRef]
196. Schwartz, B.J.; Peteanu, L.A.; Harris, C.B. Direct Observation of Fast Proton Transfer: Femtosecond Photophysics of 3-Hydroxyflavone. *J. Phys. Chem.* **1992**, *96*, 3591–3598. [CrossRef]
197. Ameer-Beg, S.; Ormson, S.M.; Brown, R.G.; Matousek, P.; Towrie, M.; Nibbering, E.T.J.; Foggi, P.; Neuwahl, F.V.R. Ultrafast Measurements of Excited State Intramolecular Proton Transfer (ESIPT) in Room Temperature Solutions of 3-Hydroxyflavone and Derivatives. *J. Phys. Chem. A* **2001**, *105*, 3709–3718. [CrossRef]
198. Roshal, A.D.; Grigorovich, A.V.; Doroshenko, A.O.; Pivovarenko, V.G.; Demchenko, A.P. Flavonols as Metal-Ion Chelators: Complex Formation with Mg2+ and Ba2+ Cations in the Excited State. *J. Photochem. Photobiol. A Chem.* **1999**, *127*, 89–100. [CrossRef]
199. Smith, G.J.; Markham, K.R. Tautomerism of Flavonol Glucosides: Relevance to Plant UV Protection and Flower Colour. *J. Photochem. Photobiol. A Chem.* **1998**, *118*, 99–105. [CrossRef]
200. Feng, W.; Wang, Y.; Chen, S.; Wang, C.; Wang, S.; Li, S.; Li, H.; Zhou, G.; Zhang, J. 4-Nitroimidazole-3-Hydroxyflavone Conjugate as a Fluorescent Probe for Hypoxic Cells. *Dye. Pigment.* **2016**, *131*, 145–153. [CrossRef]
201. Dyrager, C.; Friberg, A.; Dahlén, K.; Fridén-Saxin, M.; Börjesson, K.; Wilhelmsson, L.M.; Smedh, M.; Grøtli, M.; Luthman, K. 2,6,8-Trisubstituted 3-Hydroxychromone Derivatives as Fluorophores for Live-Cell Imaging. *Chem.–Eur. J.* **2009**, *15*, 9417–9423. [CrossRef]
202. Chen, S.; Hou, P.; Zhou, B.; Song, X.; Wu, J.; Zhang, H.; Foley, J.W. A Red Fluorescent Probe for Thiols Based on 3-Hydroxyflavone and Its Application in Living Cell Imaging. *RSC Adv.* **2013**, *3*, 11543–11546. [CrossRef]
203. Liu, B.; Luo, Z.; Si, S.; Zhou, X.; Pan, C.; Wang, L. A Photostable Triphenylamine-Based Flavonoid Dye: Solvatochromism, Aggregation-Induced Emission Enhancement, Fabrication of Organic Nanodots, and Cell Imaging Applications. *Dye. Pigment.* **2017**, *142*, 32–38. [CrossRef]
204. Dong, L.-Y.; Wang, L.-Y.; Wang, X.-F.; Liu, Y.; Liu, H.-L.; Xie, M.-X. Development of Fluorescent FRET Probe for Determination of Glucose Based on β-Cyclodextrin Modified ZnS-Quantum Dots and Natural Pigment 3-Hydroxyflavone. *Dye. Pigment.* **2016**, *128*, 170–178. [CrossRef]
205. Tomin, V.I.; Ushakou, D.V. Use of 3-Hydroxyflavone as a Fluorescence Probe for the Controlled Photopolymerization of the E-Shell 300 Polymer. *Polym. Test.* **2017**, *64*, 77–82. [CrossRef]
206. Woolfe, G.J.; Thistlethwaite, P.J. Direct Observation of Excited State Intramolecular Proton Transfer Kinetics in 3-Hydroxyflavone. *J. Am. Chem. Soc.* **1981**, *103*, 6916–6923. [CrossRef]
207. Itoh, M.; Tokumura, K.; Tanimoto, Y.; Okada, Y.; Takeuchi, H.; Obi, K.; Tanaka, I. Time-Resolved and Steady-State Fluorescence Studies of the Excited-State Proton Transfer in 3-Hydroxyflavone and 3-Hydroxychromone. *J. Am. Chem. Soc.* **1982**, *104*, 4146–4150. [CrossRef]
208. Itoh, M.; Fujiwara, Y. Two-Step Laser Excitation Fluorescence Study of the Ground- and Excited-State Proton Transfer in 3-Hydroxyflavone and 3-Hydroxychromone. *J. Phys. Chem.* **1983**, *87*, 4558–4560. [CrossRef]
209. Ernsting, N.P.; Dick, B. Fluorescence Excitation of Isolated, Jet-Cooled 3-Hydroxyflavone: The Rate of Excited State Intramolecular Proton Transfer from Homogeneous Linewidths. *Chem. Phys.* **1989**, *136*, 181–186. [CrossRef]
210. Sarkar, M.; Sengupta, P.K. Influence of Different Micellar Environments on the Excited-State Proton-Transfer Luminescence of 3-Hydroxyflavone. *Chem. Phys. Lett.* **1991**, *179*, 68–72. [CrossRef]
211. Dick, B. AM1 and INDO/S Calculations on Electronic Singlet and Triplet States Involved in Excited-State Intramolecular Proton Transfer of 3-Hydroxyflavone. *J. Phys. Chem.* **1990**, *94*, 5752–5756. [CrossRef]
212. Ramešová, Š.; Sokolová, R.; Degano, I. The Study of the Oxidation of the Natural Flavonol Fisetin Confirmed Quercetin Oxidation Mechanism. *Electrochim. Acta* **2015**, *182*, 544–549. [CrossRef]
213. Pietta, P.-G. Flavonoids as Antioxidants. *J. Nat. Prod.* **2000**, *63*, 1035–1042. [CrossRef] [PubMed]
214. Agati, G.; Azzarello, E.; Pollastri, S.; Tattini, M. Flavonoids as Antioxidants in Plants: Location and Functional Significance. *Plant Sci.* **2012**, *196*, 67–76. [CrossRef] [PubMed]
215. Martinez, M.L.; Studer, S.L.; Chou, P.T. Direct Evidence of the Triplet-State Origin of the Slow Reverse Proton Transfer Reaction of 3-Hydroxyflavone. *J. Am. Chem. Soc.* **1990**, *112*, 2427–2429. [CrossRef]
216. Yokoe, I.; Higuchi, K.; Shirataki, Y.; Komatsu, M. Photochemistry of Flavonoids. III. Photorearrangement of Flavonols. *Chem. Pharm. Bull.* **1981**, *29*, 894–898. [CrossRef]
217. Matsuura, T.; Takemoto, T.; Nakashima, R. Photoinduced Reactions—LXXI: Photorearrangement of 3-Hydroxyflavones to 3-Aryl-3-Hydroxy-1,2-Indandiones. *Tetrahedron* **1973**, *29*, 3337–3340. [CrossRef]
218. Tehfe, M.-A.; Lalevée, J.; Morlet-Savary, F.; Graff, B.; Blanchard, N.; Fouassier, J.-P. Tunable Organophotocatalysts for Polymerization Reactions Under Visible Lights. *Macromolecules* **2012**, *45*, 1746–1752. [CrossRef]

219. Lalevée, J.; Tehfe, M.-A.; Zein-Fakih, A.; Ball, B.; Telitel, S.; Morlet-Savary, F.; Graff, B.; Fouassier, J.P. N-Vinylcarbazole: An Additive for Free Radical Promoted Cationic Polymerization upon Visible Light. *ACS Macro Lett.* **2012**, *1*, 802–806. [CrossRef]
220. Condat, M.; Babinot, J.; Tomane, S.; Malval, J.-P.; Kang, I.-K.; Spillebout, F.; Mazeran, P.-E.; Lalevée, J.; Andalloussi, S.A.; Versace, D.-L. Development of Photoactivable Glycerol-Based Coatings Containing Quercetin for Antibacterial Applications. *RSC Adv.* **2016**, *6*, 18235–18245. [CrossRef]
221. Niedre, M.J.; Secord, A.J.; Patterson, M.S.; Wilson, B.C. In Vitro Tests of the Validity of Singlet Oxygen Luminescence Measurements as a Dose Metric in Photodynamic Therapy. *Cancer Res.* **2003**, *63*, 7986–7994.
222. Ragàs, X.; Cooper, L.P.; White, J.H.; Nonell, S.; Flors, C. Quantification of Photosensitized Singlet Oxygen Production by a Fluorescent Protein. *ChemPhysChem* **2011**, *12*, 161–165. [CrossRef]
223. Ragàs, X.; Agut, M.; Nonell, S. Singlet Oxygen in Escherichia Coli: New Insights for Antimicrobial Photodynamic Therapy. *Free Radic. Biol. Med.* **2010**, *49*, 770–776. [CrossRef] [PubMed]
224. Cahan, R.; Schwartz, R.; Langzam, Y.; Nitzan, Y. Light-Activated Antibacterial Surfaces Comprise Photosensitizers. *Photochem. Photobiol.* **2011**, *87*, 1379–1386. [CrossRef] [PubMed]
225. Oh, K.W.; Choi, H.-M.; Kim, J.M.; Park, J.H.; Park, I.S. A Novel Antimicrobial Photosensitizer: Hydroxyethyl Michler's Ketone. *Text. Res. J.* **2014**, *84*, 808–818. [CrossRef]
226. Freire, F.; Costa, A.C.B.P.; Pereira, C.A.; Beltrame Junior, M.; Junqueira, J.C.; Jorge, A.O.C. Comparison of the Effect of Rose Bengal- and Eosin Y-Mediated Photodynamic Inactivation on Planktonic Cells and Biofilms of Candida Albicans. *Lasers Med. Sci.* **2014**, *29*, 949–955. [CrossRef] [PubMed]
227. Guo, Y.; Rogelj, S.; Zhang, P. Rose Bengal-Decorated Silica Nanoparticles as Photosensitizers for Inactivation of Gram-Positive Bacteria. *Nanotechnology* **2010**, *21*, 065102. [CrossRef] [PubMed]
228. Felgenträger, A.; Maisch, T.; Späth, A.; Schröder, J.A.; Bäumler, W. Singlet Oxygen Generation in Porphyrin-Doped Polymeric Surface Coating Enables Antimicrobial Effects on Staphylococcus Aureus. *Phys. Chem. Chem. Phys.* **2014**, *16*, 20598–20607. [CrossRef]
229. Yano, S.; Hirohara, S.; Obata, M.; Hagiya, Y.; Ogura, S.; Ikeda, A.; Kataoka, H.; Tanaka, M.; Joh, T. Current States and Future Views in Photodynamic Therapy. *J. Photochem. Photobiol. C Photochem. Rev.* **2011**, *12*, 46–67. [CrossRef]
230. Cohn, G.E.; Tseng, H.Y. Photodynamic Inactivation of Yeast Sensitized by Eosin Y. *Photochem. Photobiol.* **1977**, *26*, 465–474. [CrossRef]
231. Usacheva, M.N.; Teichert, M.C.; Biel, M.A. Comparison of the Methylene Blue and Toluidine Blue Photobactericidal Efficacy against Gram-Positive and Gram-Negative Microorganisms. *Lasers Surg. Med.* **2001**, *29*, 165–173. [CrossRef]
232. Bovis, M.J.; Noimark, S.; Woodhams, J.H.; Kay, C.W.M.; Weiner, J.; Peveler, W.J.; Correia, A.; Wilson, M.; Allan, E.; Parkin, I.P.; et al. Photosensitisation Studies of Silicone Polymer Doped with Methylene Blue and Nanogold for Antimicrobial Applications. *RSC Adv.* **2015**, *5*, 54830–54842. [CrossRef]
233. Araújo, P.V.; Teixeira, K.I.R.; Lanza, L.D.; Cortes, M.E.; Poletto, L.T.A. In Vitro Lethal Photosensitization of S. Mutans Using Methylene Blue and Toluidine Blue o as Photosensitizers. *Acta Odontológica Latinoam.* **2009**, *22*, 93–97.
234. David, A.; Arulmoli, R.; Parasuraman, S.; Parasuraman, S. Overviews of Biological Importance of Quercetin: A Bioactive Flavonoid. *Pharmacogn. Rev.* **2016**, *10*, 84–89. [CrossRef]
235. Baranowska, M.; Koziara, Z.; Suliborska, K.; Chrzanowski, W.; Wormstone, M.; Namieśnik, J.; Bartoszek, A. Interactions between Polyphenolic Antioxidants Quercetin and Naringenin Dictate the Distinctive Redox-Related Chemical and Biological Behaviour of Their Mixtures. *Sci. Rep.* **2021**, *11*, 12282. [CrossRef] [PubMed]
236. Nair, M.P.; Mahajan, S.; Reynolds, J.L.; Aalinkeel, R.; Nair, H.; Schwartz, S.A.; Kandaswami, C. The Flavonoid Quercetin Inhibits Proinflammatory Cytokine (Tumor Necrosis Factor Alpha) Gene Expression in Normal Peripheral Blood Mononuclear Cells via Modulation of the NF-Kβ System. *Clin. Vaccine Immunol.* **2006**, *13*, 319–328. [CrossRef] [PubMed]
237. Batiha, G.E.; Beshbishy, A.M.; Ikram, M.; Mulla, Z.S.; El-Hack, M.E.A.; Taha, A.E.; Algammal, A.M.; Elewa, Y.H. The Pharmacological Activity, Biochemical Properties, and Pharmacokinetics of the Major Natural Polyphenolic Flavonoid: Quercetin. *Foods* **2020**, *9*, 374. [CrossRef] [PubMed]
238. Russo, M.; Spagnuolo, C.; Tedesco, I.; Bilotto, S.; Russo, G.L. The Flavonoid Quercetin in Disease Prevention and Therapy: Facts and Fancies. *Biochem. Pharmacol.* **2012**, *83*, 6–15. [CrossRef] [PubMed]
239. Sokolová, R.; Ramešová, Š.; Degano, I.; Hromadová, M.; Gál, M.; Žabka, J. The Oxidation of Natural Flavonoid Quercetin. *Chem. Commun.* **2012**, *48*, 3433–3435. [CrossRef] [PubMed]
240. Hertog, M.G.; Hollman, P.C. Potential Health Effects of the Dietary Flavonol Quercetin. *Eur. J. Clin. Nutr.* **1996**, *50*, 63–71.
241. Erden Inal, M.; Kahraman, A.; Köken, T. Beneficial Effects of Quercetin on Oxidative Stress Induced by Ultraviolet A. *Clin. Exp. Dermatol.* **2001**, *26*, 536–539. [CrossRef]
242. Sestili, P.; Guidarelli, A.; Dachà, M.; Cantoni, O. Quercetin Prevents DNA Single Strand Breakage and Cytotoxicity Caused By Tert-Butylhydroperoxide: Free Radical Scavenging Versus Iron Chelating Mechanism. *Free Radic. Biol. Med.* **1998**, *25*, 196–200. [CrossRef]
243. Brown, J.P. A Review of the Genetic Effects of Naturally Occurring Flavonoids, Anthraquinones and Related Compounds. *Mutat. Res./Rev. Genet. Toxicol.* **1980**, *75*, 243–277. [CrossRef] [PubMed]

244. Read, M.A. Flavonoids: Naturally Occurring Anti-Inflammatory Agents. *Am. J. Pathol.* **1995**, *147*, 235–237. [PubMed]
245. Ohnishi, E.; Bannai, H. Quercetin Potentiates TNF-Induced Antiviral Activity. *Antivir. Res.* **1993**, *22*, 327–331. [CrossRef] [PubMed]
246. Zhu, D.; Peng, X.; Xiao, P. Penta-Hydroxy Flavones-Based Photoinitiating Systems for Free Radical, Cationic, and Thiol-Ene Polymerization upon Exposure to Mild Blue LEDs. *Macromol. Mater. Eng.* **2021**, *306*, 2100059. [CrossRef]
247. Lee, J.; Jin, H.; Lee, W.S.; Nagappan, A.; Choi, Y.H.; Kim, G.S.; Jung, J.; Ryu, C.H.; Shin, S.C.; Hong, S.C.; et al. Morin, a Flavonoid from Moraceae, Inhibits Cancer Cell Adhesion to Endothelial Cells and EMT by Downregulating VCAM1 and Ncadherin. *Asian Pac. J. Cancer Prev.* **2016**, *17*, 3071–3075.
248. Lee, Y.J.; Kim, W.I.; Kim, S.Y.; Cho, S.W.; Nam, H.S.; Lee, S.H.; Cho, M.K. Flavonoid Morin Inhibits Proliferation and Induces Apoptosis of Melanoma Cells by Regulating Reactive Oxygen Species, Sp1 and Mcl-1. *Arch. Pharmacal Res.* **2019**, *42*, 531–542. [CrossRef] [PubMed]
249. Rajput, S.A.; Wang, X.; Yan, H.-C. Morin Hydrate: A Comprehensive Review on Novel Natural Dietary Bioactive Compound with Versatile Biological and Pharmacological Potential. *Biomed. Pharmacother.* **2021**, *138*, 111511. [CrossRef]
250. Olayinka, E.T.; Ore, A.; Adeyemo, O.A.; Ola, O.S. The Role of Flavonoid Antioxidant, Morin in Improving Procarbazine-Induced Oxidative Stress on Testicular Function in Rat. *Porto Biomed. J.* **2019**, *4*, e28. [CrossRef]
251. Matsumoto, A. Polymerization of Multiallyl Monomers. *Prog. Polym. Sci.* **2001**, *26*, 189–257. [CrossRef]
252. Hoyle, C.E.; Lee, T.Y.; Roper, T. Thiol–Enes: Chemistry of the Past with Promise for the Future. *J. Polym. Sci. Part A Polym. Chem.* **2004**, *42*, 5301–5338. [CrossRef]
253. Hata, E.; Mitsube, K.; Momose, K.; Tomita, Y. Holographic Nanoparticle-Polymer Composites Based on Step-Growth Thiol-Ene Photopolymerization. *Opt. Mater. Express* **2011**, *1*, 207–222. [CrossRef]
254. Al Mousawi, A.; Garra, P.; Schmitt, M.; Toufaily, J.; Hamieh, T.; Graff, B.; Fouassier, J.P.; Dumur, F.; Lalevée, J. 3-Hydroxyflavone and N-Phenylglycine in High Performance Photoinitiating Systems for 3D Printing and Photocomposites Synthesis. *Macromolecules* **2018**, *51*, 4633–4641. [CrossRef]
255. Garra, P.; Graff, B.; Morlet-Savary, F.; Dietlin, C.; Becht, J.-M.; Fouassier, J.-P.; Lalevée, J. Charge Transfer Complexes as Pan-Scaled Photoinitiating Systems: From 50 Mm 3D Printed Polymers at 405 Nm to Extremely Deep Photopolymerization (31 Cm). *Macromolecules* **2018**, *51*, 57–70. [CrossRef]
256. Bonifačić, M.; Štefanić, I.; Hug, G.L.; Armstrong, D.A.; Asmus, K.-D. Glycine Decarboxylation: The Free Radical Mechanism. *J. Am. Chem. Soc.* **1998**, *120*, 9930–9940. [CrossRef]
257. Ullrich, G.; Burtscher, P.; Salz, U.; Moszner, N.; Liska, R. Phenylglycine Derivatives as Coinitiators for the Radical Photopolymerization of Acidic Aqueous Formulations. *J. Polym. Sci. Part A Polym. Chem.* **2006**, *44*, 115–125. [CrossRef]
258. You, J.; Fu, H.; Zhao, D.; Hu, T.; Nie, J.; Wang, T. Flavonol Dyes with Different Substituents in Photopolymerization. *J. Photochem. Photobiol. A Chem.* **2020**, *386*, 112097. [CrossRef]
259. You, J.; Cao, D.; Hu, T.; Ye, Y.; Jia, X.; Li, H.; Hu, X.; Dong, Y.; Ma, Y.; Wang, T. Novel Norrish Type I Flavonoid Photoinitiator for Safe LED Light with High Activity and Low Toxicity by Inhibiting the ESIPT Process. *Dye. Pigment.* **2021**, *184*, 108865. [CrossRef]
260. You, J.; Du, Y.; Xue, T.; Bao, B.; Hu, T.; Ye, Y.; Wang, T. The Three-Component Photoinitiating Systems Based on Flavonol Sulfonate and Application in 3D Printing. *Dye. Pigment.* **2022**, *197*, 109899. [CrossRef]
261. Chen, H.; Regeard, C.; Salmi, H.; Morlet-Savary, F.; Giacoletto, N.; Nechab, M.; Xiao, P.; Dumur, F.; Lalevée, J. Interpenetrating Polymer Network Hydrogels Using Natural Based Dyes Initiating Systems: Antibacterial Activity and 3D/4D Performance. *Eur. Polym. J.* **2022**, *166*, 111042. [CrossRef]
262. Chen, H.; Noirbent, G.; Zhang, Y.; Brunel, D.; Gigmes, D.; Morlet-Savary, F.; Graff, B.; Xiao, P.; Dumur, F.; Lalevée, J. Novel D–π-A and A–π-D–π-A Three-Component Photoinitiating Systems Based on Carbazole/Triphenylamino Based Chalcones and Application in 3D and 4D Printing. *Polym. Chem.* **2020**, *11*, 6512–6528. [CrossRef]
263. Li, M.; Du, Y.; Zhan, H.; Zhang, L.; Wu, H.; Zhao, D.; Wang, Q.; Wang, T. Synthesis and Photochemistry of Flavonol Camphorsulfonates Photoinitiator with Different Substituents. *Prog. Org. Coat.* **2023**, *183*, 107810. [CrossRef]
264. Brahmachari, G.; Nurjamal, K.; Karmakar, I.; Mandal, M. Camphor-10-Sulfonic Acid (CSA): A Water Compatible Organocatalyst in Organic Transformations. *Curr. Organocatal.* **2018**, *5*, 165–181. [CrossRef]
265. Fehr, M.; Appl, Á.; Esdaile, D.J.; Naumann, S.; Schulz, M.; Dahms, I. D-10-Camphorsulfonic Acid: Safety Evaluation. *Mutat. Res./Genet. Toxicol. Environ. Mutagen.* **2020**, *858–860*, 503257. [CrossRef]
266. Andraos, J.; Barclay, G.G.; Medeiros, D.R.; Baldovi, M.V.; Scaiano, J.C.; Sinta, R. Model Studies on the Photochemistry of Phenolic Sulfonate Photoacid Generators. *Chem. Mater.* **1998**, *10*, 1694–1699. [CrossRef]
267. He, B.-H.; He, J.; Wang, G.-X.; Liu, L.-C.; Wu, H.; Zhong, M. Photoinduced Controlled/"Living" Polymerization of Methyl Methacrylate with Flavone as Photoinitiator. *J. Appl. Polym. Sci.* **2016**, *133*, 43845. [CrossRef]
268. Al Mousawi, A.; Garra, P.; Dumur, F.; Graff, B.; Fouassier, J.P.; Lalevée, J. Flavones as Natural Photoinitiators for Light Mediated Free-Radical Polymerization via Light Emitting Diodes. *J. Polym. Sci.* **2020**, *58*, 254–262. [CrossRef]
269. Miean, K.H.; Mohamed, S. Flavonoid (Myricetin, Quercetin, Kaempferol, Luteolin, and Apigenin) Content of Edible Tropical Plants. *J. Agric. Food Chem.* **2001**, *49*, 3106–3112. [CrossRef]

270. Walle, T.; Otake, Y.; Brubaker, J.A.; Walle, U.K.; Halushka, P.V. Disposition and Metabolism of the Flavonoid Chrysin in Normal Volunteers. *Br. J. Clin. Pharmacol.* **2001**, *51*, 143–146. [CrossRef]
271. Jana, K.; Yin, X.; Schiffer, R.B.; Chen, J.-J.; Pandey, A.K.; Stocco, D.M.; Grammas, P.; Wang, X. Chrysin, a Natural Flavonoid Enhances Steroidogenesis and Steroidogenic Acute Regulatory Protein Gene Expression in Mouse Leydig Cells. *J. Endocrinol.* **2008**, *197*, 315–323. [CrossRef]
272. Oliveira, G.A.R.; Ferraz, E.R.A.; Souza, A.O.; Lourenço, R.A.; Oliveira, D.P.; Dorta, D.J. Evaluation of the Mutagenic Activity of Chrysin, a Flavonoid Inhibitor of the Aromatization Process. *J. Toxicol. Environ. Health Part A* **2012**, *75*, 1000–1011. [CrossRef]
273. Manzolli, E.S.; Serpeloni, J.M.; Grotto, D.; Bastos, J.K.; Antunes, L.M.G.; Barbosa, F.; Barcelos, G.R.M. Protective Effects of the Flavonoid Chrysin against Methylmercury-Induced Genotoxicity and Alterations of Antioxidant Status, In Vivo. *Oxidative Med. Cell. Longev.* **2015**, *2015*, 602360. [CrossRef]
274. Flores-Aguilar, L.Á.; Cueto-Escobedo, J.; Puga-Olguín, A.; Olmos-Vázquez, O.J.; Rosas-Sánchez, G.U.; Bernal-Morales, B.; Rodríguez-Landa, J.F. Behavioral Despair Is Blocked by the Flavonoid Chrysin (5,7-Dihydroxyflavone) in a Rat Model of Surgical Menopause. *Molecules* **2023**, *28*, 587. [CrossRef]
275. Lin, C.C.; Yu, C.S.; Yang, J.S.; Lu, C.C.; Chiang, J.H.; Lin, J.P.; Kuo, C.-L.; Chung, J.G. Chrysin, a Natural and Biologically Active Flavonoid, Influences a Murine Leukemia Model In Vivo through Enhancing Populations of T-and B-Cells, and Promoting Macrophage Phagocytosis and NK Cell Cytotoxicity. *In Vivo* **2012**, *26*, 665.
276. Mohos, V.; Fliszár-Nyúl, E.; Ungvári, O.; Bakos, É.; Kuffa, K.; Bencsik, T.; Zsidó, B.Z.; Hetényi, C.; Telbisz, Á.; Özvegy-Laczka, C.; et al. Effects of Chrysin and Its Major Conjugated Metabolites Chrysin-7-Sulfate and Chrysin-7-Glucuronide on Cytochrome P450 Enzymes and on OATP, P-Gp, BCRP, and MRP2 Transporters. *Drug Metab Dispos* **2020**, *48*, 1064. [CrossRef]
277. Huang, J.; Yves Le Gac, P.; Richaud, E. Thermal Oxidation of Poly(Dicyclopentadiene)-Effect of Phenolic and Hindered Amine Stabilizers. *Polym. Degrad. Stab.* **2021**, *183*, 109267. [CrossRef]
278. Pavlinec, J.; Kleinová, A.; Moszner, N. The Depletion of Substituted Phenolic Stabilizers by Conjugate C-Addition to Acrylic Monomers in Multicomponent Systems. *Macromol. Mater. Eng.* **2012**, *297*, 1005–1013. [CrossRef]
279. Bouzrati-Zerelli, M.; Maier, M.; Fik, C.P.; Dietlin, C.; Morlet-Savary, F.; Fouassier, J.P.; Klee, J.E.; Lalevée, J. A Low Migration Phosphine to Overcome the Oxygen Inhibition in New High Performance Photoinitiating Systems for Photocurable Dental Type Resins. *Polym. Int.* **2017**, *66*, 504–511. [CrossRef]
280. Courtecuisse, F.; Belbakra, A.; Croutxé-Barghorn, C.; Allonas, X.; Dietlin, C. Zirconium Complexes to Overcome Oxygen Inhibition in Free-Radical Photopolymerization of Acrylates: Kinetic, Mechanism, and Depth Profiling. *J. Polym. Sci. Part A Polym. Chem.* **2011**, *49*, 5169–5175. [CrossRef]
281. Xu, F.; Yang, J.-L.; Gong, Y.-S.; Ma, G.-P.; Nie, J. A Fluorinated Photoinitiator for Surface Oxygen Inhibition Resistance. *Macromolecules* **2012**, *45*, 1158–1164. [CrossRef]
282. Yang, Q.; Lalevée, J.; Poly, J. Development of a Robust Photocatalyzed ATRP Mechanism Exhibiting Good Tolerance to Oxygen and Inhibitors. *Macromolecules* **2016**, *49*, 7653–7666. [CrossRef]
283. Yeow, J.; Shanmugam, S.; Corrigan, N.; Kuchel, R.P.; Xu, J.; Boyer, C. A Polymerization-Induced Self-Assembly Approach to Nanoparticles Loaded with Singlet Oxygen Generators. *Macromolecules* **2016**, *49*, 7277–7285. [CrossRef]
284. Kirschner, J.; Becht, J.-M.; Klee, J.E.; Lalevée, J. A New Phosphine for Efficient Free Radical Polymerization under Air. *Macromol. Rapid Commun.* **2020**, *41*, 2000053. [CrossRef] [PubMed]
285. Dietlin, C.; Trinh, T.T.; Schweizer, S.; Graff, B.; Morlet-Savary, F.; Noirot, P.-A.; Lalevée, J. New Phosphine Oxides as High Performance Near- UV Type I Photoinitiators of Radical Polymerization. *Molecules* **2020**, *25*, 1671. [CrossRef] [PubMed]
286. Abdul-Monem, M.M. Naturally Derived Photoinitiators for Dental and Biomaterials Applications. *Eur. Dent. Res. Biomater. J.* **2021**, *1*, 72–78. [CrossRef]
287. Limtrakul, P.; Semmarath, W.; Mapoung, S. Anthocyanins and Proanthocyanidins in Natural Pigmented Rice and Their Bioactivities. In *Phytochemicals in Human Health*; Rao, V., Mans, D., Rao, L., Eds.; IntechOpen: Rijeka, Croatia, 2019; Chapter 1; ISBN 978-1-78985-588-3.
288. Mannino, G.; Chinigò, G.; Serio, G.; Genova, T.; Gentile, C.; Munaron, L.; Bertea, C.M. Proanthocyanidins and Where to Find Them: A Meta-Analytic Approach to Investigate Their Chemistry, Biosynthesis, Distribution, and Effect on Human Health. *Antioxidants* **2021**, *10*, 1229. [CrossRef] [PubMed]
289. Rauf, A.; Imran, M.; Abu-Izneid, T.; Iahtisham-Ul-Haq; Patel, S.; Pan, X.; Naz, S.; Sanches Silva, A.; Saeed, F.; Rasul Suleria, H.A. Proanthocyanidins: A Comprehensive Review. *Biomed. Pharmacother.* **2019**, *116*, 108999. [CrossRef]
290. Nie, Y.; Stürzenbaum, S.R. Proanthocyanidins of Natural Origin: Molecular Mechanisms and Implications for Lipid Disorder and Aging-Associated Diseases. *Adv. Nutr.* **2019**, *10*, 464–478. [CrossRef]
291. Nie, F.; Liu, L.; Cui, J.; Zhao, Y.; Zhang, D.; Zhou, D.; Wu, J.; Li, B.; Wang, T.; Li, M.; et al. Oligomeric Proanthocyanidins: An Updated Review of Their Natural Sources, Synthesis, and Potentials. *Antioxidants* **2023**, *12*, 1004. [CrossRef]
292. Dixon, R.A.; Xie, D.-Y.; Sharma, S.B. Proanthocyanidins–a Final Frontier in Flavonoid Research? *New Phytol.* **2005**, *165*, 9–28. [CrossRef]
293. Yang, K.; Chan, C.B. Proposed Mechanisms of the Effects of Proanthocyanidins on Glucose Homeostasis. *Nutr. Rev.* **2017**, *75*, 642–657. [CrossRef]

294. Hass, V.; Li, Y.; Wang, R.; Nguyen, D.; Peng, Z.; Wang, Y. Methacrylate-Functionalized Proanthocyanidins as Novel Polymerizable Collagen Cross-Linkers–Part 1: Efficacy in Dentin Collagen Bio-Stabilization and Cross-Linking. *Dent. Mater.* **2021**, *37*, 1183–1192. [CrossRef] [PubMed]
295. Wang, R.; Li, Y.; Hass, V.; Peng, Z.; Wang, Y. Methacrylate-Functionalized Proanthocyanidins as Novel Polymerizable Collagen Cross-Linkers—Part 2: Effects on Polymerization, Microhardness and Leaching of Adhesives. *Dent. Mater.* **2021**, *37*, 1193–1201. [CrossRef] [PubMed]